Materials Advances

REVIEW

Bubble-propelled micro/nanomotors: a robust platform for the detection of environmental pollutants and biosensing

Suvendu Kumar Panda, [ID] [a] Nomaan Alam Kherani, [ID] [b] Srikanta Debata [ID] [a] and Dhruv Pratap Singh [ID] *[a]

The sensitive and rapid detection of a variety of hazardous environmental pollutants and bio-analytes such as microorganisms and biomolecules is of great importance for environmental and health care monitoring. Thus, significant progress has been made in the development of numerous sensor platforms for the quick and reliable sensitive detection of these analytes. However, most of the sensor platforms require complex technology, skillful personnel, prolonged operation, and laborious protocols, which limit their use worldwide, especially in low- and middle-income countries. Over the past few decades, the emergence and progress of nanotechnology have revolutionized the field of sensing. Particularly, the birth of self-propelled micro/nanomotors has become an area of interest in the current era owing to their versatility, ranging from environmental monitoring to biosensing. These are synthetic tiny multifunctional intelligent systems, capable of converting external energy such as light, magnetic field, ultrasound, electric field, and chemical fuel to kinetic energy and accomplishing tedious jobs. Among the external driving sources, chemically driven micromotors based on the bubble propulsion mechanism hold considerable promise in sensing on account of their greater propulsion rate, enhanced fluid mixing, and mass transfer. Employing this advantage, many leading research groups have focused on the fabrication of differently shaped bubble-propelled micromotors for the sensitive and selective detection of targets by functionalizing the motors with specific recognition units. In this review, we highlight the current progress in bubble-propelled micro/nanomotors for the detection of various environmental pollutants and bioanalytes such as microorganisms, cells, and biomolecules, and discuss their sensing mechanism. Finally, the challenges and limitations of these micromotors are presented together with their future direction.

a Department of Physics, IIT Bhilai, GEC Campus, Sejbahar, Raipur, Chhattisgarh, 492015, India. E-mail: dhruv@iitbhilai.ac.in
b Department of EECS, IIT Bhilai, GEC Campus, Sejbahar, Raipur, Chhattisgarh, 492015, India

Suvendu Kumar Panda is a PhD scholar at the Department of Physics, Indian Institute of Technology (IIT) Bhilai. He graduated with a B.Sc. in Physics from Fakir Mohan University, Odisha, India. He completed his Master's Degree in Condensed Matter Physics from Sambalpur University, India. As a research scholar, he is currently working on active colloidal systems and studying their dynamics in different fluid mediums. His research interest includes the fabrication of different shapes of micro/nanomotors and their use in biomedical applications and environmental remediation.

Suvendu Kumar Panda

Nomaan Alam Kherani is currently an Electrical Engineering undergraduate at the Indian Institute of Technology (IIT-Bhilai). His research activities include queueing theory, machine learning, and integration of satellite and terrestrial networks and micro/nanomotors.

Nomaan Alam Kherani

1. Introduction

Almost all living organisms are composed primarily of water, a basic and essential ingredient to drive the body. However, presently, the rapid industrialization has led to the emission of chemical wastes and their by-products into freshwater bodies. This has resulted in an increase in the amount of hazardous pollutants in water bodies, which has a devastating effect on aquatic ecosystems and seriously impact of human health, causing many waterborne diseases and neurological, hematological, and dermatological disorders.[1–3] Given that the bond between the environment and human biology is inseparable, both environmental pollutants and biological analytes should be detected regularly to ensure environmental pollutants monitoring and health care protection through the early-stage diagnosis of various diseases. In addition, the current age is witnessing many chronic ailments such as cancer and tumors not only due to the exposure to environmental and biological pollutants such as heavy metal ions, chemical warfare agents (CWA), explosives, toxic gases, and micropathogens but also due to unhealthy lifestyle, consumption of fertilizer-based unhygienic foods, *etc.* Thus, collaborative efforts from both environment and health agencies have emphasized the quantitative measurement and detection of environmental pollutants and biohazards such as microorganisms, tumor cells, and biomolecules in water, food, and in the body.[4,5] However, the traditional and early methods for the detection of these toxic analytes are based on sophisticated and costly instrumentation, generally requiring skilled technicians and a long operational period.[4] Although these methods give accurate results, their use in underdeveloped and developing countries is limited due to the lack of funding, biomedical facilities, and skillful personnel. Thus, to solve the above-mentioned problems, researchers have devoted their efforts to the development of cost-effective and facile sensing probes with improved sensitivity and selectivity. Over the past few decades, the emergence and progress of nanofabrication and design have revolutionized the field of sensing.[6–12] In particular, the utilization of micro/nanomaterials as a sensing tool has miniaturized the size of sensors, exhibiting potential for good resolution with minimal efforts and reduced operation time by eliminating the demand for costly and powerful setups. However, although these micro/nanomaterials exhibit beneficial optical and electrochemical detection mechanisms for the precise sensing and analysis of analytes, they cannot fulfill the current demands of localized and targeted area detection.

Currently, the innovation of self-propelled micromotors has become an area of interest owing to their practical applicability in many fields ranging from environmental monitoring to biosensing.[13–18] The dominance of these micromotors over the micro/nanoparticles is due to their ability to exhibit autonomous motion through chemical or physical reactions, which results in the enhanced micromixing of fluids, guaranteeing the interaction between the functional probes and target analytes. Consequently, the performance and accuracy of sensing are tremendously escalated at the local site. Self-propelled micromotors can drive themselves in a fluid medium by harnessing external energy sources such as light,[19–22] electric field,[23–25] acoustic waves,[26,27] magnetic field,[28–30] and the surrounding chemical fuel.[31–34] Furthermore, to expand their practical utility, they are fabricated and functionalized with different materials, chemicals, and target recognition units to achieve various needs. Engineered micromotors can swim freely and perform specific jobs in a low Reynolds number regime owing to their inherent properties.[35] More importantly, the unique combination of locomotion features and excellent working ability has made them very special and attractive in the modern era. Hence, they show superiority in the field of environmental and biosensing. Considering current technological advancements, a plethora of research has been carried out to develop different types of micro/nano-motors to detect and bind specific toxins, pathogens, biomolecules, and biomarkers.[36–40] To accomplish this specific task in complex environments such as polluted water, blood, and serum, the micro/nano-motor community has regulated the speed of micromotors by using different energy sources and varying the concentration of chemical fuel. Besides,

Srikanta Debata

Srikanta Debata is pursuing his Doctorate in Physics at the Indian Institute of Technology (IIT) Bhilai. He obtained his Bachelor's (B.Sc.) Degree in Physics from Sambalpur University, Odisha. He then completed his Master's Degree (M.Sc.) in Nuclear Physics from Sambalpur University, India. His research interests include synthetic active matter, designing micro/nanorobots, and applications of micro/nanorobots in the field of biomedicine and environmental remediation.

Dhruv Pratap Singh

Dhruv Pratap Singh obtained his PhD in Physics from the Indian Institute of Technology Delhi (IIT-Delhi), India. He was a Postdoctoral Researcher at the Department of Materials Science and Engineering, POSTECH, South Korea, and a Postdoctoral Fellow in the Micro, Nano, and Molecular Systems group at the Max Planck Institute for Intelligent Systems (MPI-IS, Stuttgart, Germany). Currently, he is an Assistant Professor at the Department of Physics, Indian Institute of Technology Bhilai (IIT-Bhilai), India. His research interests include synthetic active matter, micro/nanomotors, microrobots, self-assembly, and microfluidics.

various swimming mechanisms of micromotors have been studied and categorized as diffusiophoresis,[41] thermophoresis,[42,43] magnetophoresis,[28,44] electrophoresis,[24,31] acoustophoresis,[27,45] and bubble propulsion.[46–50] Some of these mechanisms have been explored by researchers for sensing applications, for example, Park *et al.* recently demonstrated the utilization of noncatalytic polystyrene (PS) spheres towards biosensing using electric and magnetic fields.[51] Biotin-functionalized beads were loaded on the surface of PS spheres during electrophoretic motion and steered to sense and capture the avidin-modified cargo inside a microfluidic chamber, followed by its release. Zhang *et al.* designed a light-driven Au-WO$_3$@C Janus micromotor toward the detection of toxic pollutants such as sodium-2,6-dichloroindophenol (DCIP) and Rhodamine B (RhB).[52] The sensitivity of the micromotors was evaluated based on their moving speed. The speed of the motors was observed to be enhanced even at the low concentration of DCIP and RhB. This occurred due to the faster photocatalytic degradation of these chemicals by WO$_3$, which resulted in an enhanced diffusiophoretic effect. Consequently, the micromotors moved *via* a self-diffusiophoresis mechanism and confirmed the presence of these hazardous pollutants in the solution. Similarly, ultrasound-propelled nanomotors were programmed for the detection of intracellular miRNA *via* an "OFF–ON" fluorescent sensing mechanism.[53] However, although many efforts have been made to design mobile micro/nanosensors based on the aforesaid mechanisms, bubble propulsion has become a research focus given that it provides greater speed, promotes enhanced fluid mixing and mass transfer.[47,54,55] Employing materials such as Pt, MnO$_2$, Zn, Mg, some catalase enzymes and chemical fuels such as peroxide, the catalytic decomposition of peroxide can be promoted to create bubbles (oxygen, hydrogen), which apply a thrust to micromotors, resulting in their propulsion.[56–58] Similar to other micromotors, bubble-based motors are superior to static micro/nanoparticles when employed for different applications. Specifically, their motility provides advantages such as fast detection, scanning bigger volumes, and detection of pollutants or bio-species at very low concentrations. It has been shown in several examples that they outperform the conventional methods, for instance, Yuan *et al.* proposed a facile strategy, which used Janus capsule motors capable of sensing a type of explosive, *i.e.*, 2,4,6-trinitrotoluene (TNT), efficiently within a very short assay time, with a limit of detection (LOD) of 2.4 ng mL^{-1}.[59] In contrast, the existing methods for the detection of TNT such as mass spectroscopy,[60] surface plasmon resonance,[61] and fluorescence polarization[62] require cumbersome pre-treatment and sophisticated instrumentation, which take hours to achieve a similar limit of detection with high accuracy. Thus, the utilization of this technique not only showed a faster response towards the sensing of TNT but also surpassed the limitation posed by the conventional techniques. Besides the pollutant detection strategy, several investigations have also been performed to validate the technological dominance of bubble-based motors in biosensing. The differentiation of circulating tumor cells (CTC) from the normal cells in the blood stream is challenging

due to their low abundance. The only commercial setup available for the detection of CTC is the Cellsearch® system, in which anti-EpCAM-coated magnetic nanoparticles are used for the detection, followed by immunostaining for distinguishing CTC from normal cells.[63] However, a series of complex processing steps with strict conditions have to be performed during immunostaining, which requires much effort, time, and high cost. Thus, to alleviate this problem, Zhao *et al.* developed a cost-effective fabrication strategy to prepare Janus microrods in large quantities based on the motion-enhanced capture of CTC.[64] To test the selectivity and sensitivity of this method, the micromotors were mixed with a solution of CTC together with other cells. The bubble-based motors detected 25 cells mL^{-1} within 1 min and showed no interference with the other cells. This detection strategy demonstrated faster recognition of cells with a low LOD and exhibited high selectivity and a large recovery rate in blood samples. A detailed discussion of the utility of these motile motors for the detection of various pollutants and bioanalytes can be found in another section of this review.

This review is focused on the recent advancement of bubble-propelled micromotors in the last ten years for the sensing of environmental pollutants and biological analytes. There are four sections in this article. In the first section, we highlight the design of different-shaped bubble-propelled micromotors for the sensing of toxic pollutants and bioanalytes. In addition, the sensing mechanism is discussed. The second section is related to the detection of hazardous pollutants such as heavy metal ions, chemical warfare agents, nitroaromatic explosives, toxic gases, and other organic pollutants. Next, the additional feature of micromotors related to biosensing will be explored and explained. This section presents the valuable aspects and mechanisms for the detection of micropathogens, cells, biomolecules, and biomarkers in food, water, and biological media using micromotors. Finally, the existing challenges and future perspectives of sensing are presented.

2. Morphology and sensing mechanism

Micro/nanomotors must be functionalized with suitable chemical groups, nanoparticles, and target receptor units for the detection of hazardous pollutants and biosensing applications.[4] Besides surface functionalization, the shape and design of micromotors must be carefully engineered to ensure good propulsion and enhanced detection. In general, spherical Janus and tubular-shaped micromotors with variable sizes have been used for many applications.[16,70] The popularity of tubular micromotors in this topic is rich because of their open structure, which provides the maximum surface area for detection. However, some groups have also reported other forms of micromotors such as eccentric Janus,[54] Janus rods,[64] hexagon,[58] and jellyfish[55] for realizing a higher surface area to improve the catalytic activity and increase the speed of the sensing process. The schematic in Fig. 1 represents the various shapes of bubble-propelled micromotors that have been proposed for analytical sensing purposes.[16,54–56,58,64]

Fig. 1 Schematic of the morphology of various micromotors designed for bubble propulsion: clockwise from the top, Janus rod,[64] jellyfish,[55] hexagon,[58] eccentric Janus,[54] tube,[45,65,66] and Janus sphere.[40,56,59,67–69]

They are usually fabricated by either physical or chemical methods. Some critical reviews in the literature discuss the strategies for the fabrication of micromotors.[31,35,71]

Generally, micromotors equipped with different functional probes such as quantum dots, aptamers, proteins, DNA, and mi-RNA, for nano sensing function based on three types of detection mechanisms. They include motion-based, electrochemical, and optical sensing mechanisms (see Fig. 2).[10,38–40,72] Optical sensing includes both fluorescent and colorimetric assay techniques. In motion-based sensing, the velocity of micromotors is reduced significantly due to the attachment of the target molecules to the active site, consequently slowing down the

catalytic activity (see Fig. 2A(a)). In a few cases, the micromotor speed is seen to be improved by interacting with surrounding molecules, as shown in Fig. 2A(b). Electrochemical sensing platforms offer a broad spectrum in the qualitative and quantitative analysis of toxic gases, pollutants, biological molecules, etc. They function by converting a chemical signal to an electric signal. To strengthen the performance of the sensor, various modifications have been done to the sensing electrode and the sensing platform to improve the sensitivity and selectivity. Recently, micromotor-assisted electrochemical sensing has brought a breakthrough in the field of sensors. The mobile micromotors assist in speeding up the chemical reactions, and also fluid mixing, which generates enough electrons or ions as a by-product, followed by the rapid conversion of chemical information to electrical information via a transducer. The signal analysis is done by looking at the V–I characteristics curve, which confirms the presence of the analyte in the sample (see Fig. 2B). In the case of fluorescent-based optical sensing, the micromotor signal is either quenched, recovered, or changed (see Fig. 2C(a–c), respectively). Briefly, the quenching phenomenon is observed due to a decrease in the fluorescence signal of the fluorophores of micromotors upon the attachment of the target molecules (see Fig. 2C(a)). The recovery event is observed due to the property of the receptor and its affinity toward the target (see Fig. 2C(b)). This means that when the fluorescent receptor or recognition unit senses a specific target, it is released from the surface of the micromotors, which results in the recovery of the fluorescent signal in the solution. The change in the fluorescence signal from one color to another is associated with the ratiometric fluorescence sensing (see Fig. 2C(c)).[64] Generally, in this case, the micromotor bodies are immobilized with different types of dye molecules, which in response to a specific environment show the ratiometric phenomenon.
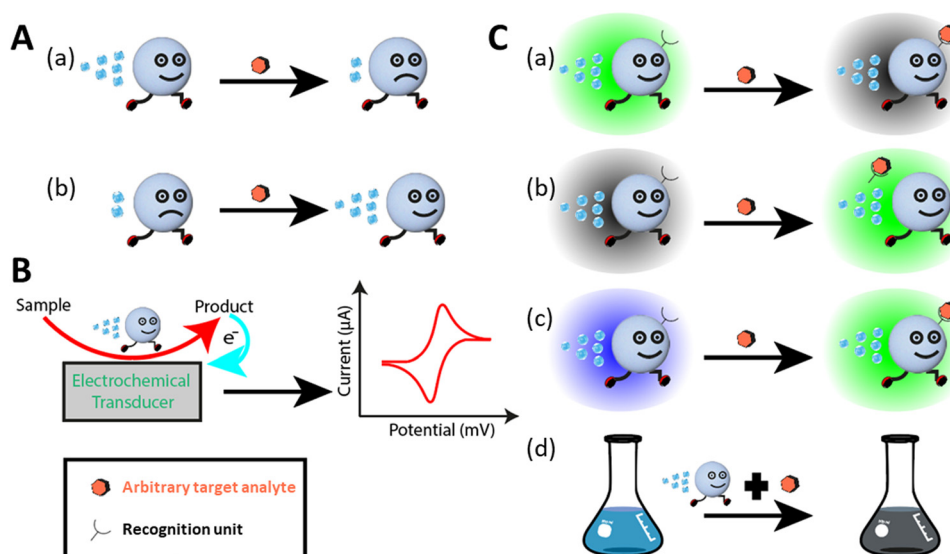

Fig. 2 Sensing mechanism. (A) Motion-based-sensing. (a and b) Decrease and increase in speed of motors upon sensing the targets. (B) Micromotor-assisted electrochemical detection. (C) Optical detection of analytes: fluorescence-based detection and colorimetric assay. (a) Fluorescence quenching. (b) Fluorescence recovery. (c) Ratiometric fluorescence response. (d) Naked-eye colorimetric assay.

Accordingly, micromotor-assisted colorimetric assays are a very cost-effective and facile technique for sample analysis within a very short time. Given that the body of micromotor is made up of different materials, it aids in the production of certain compounds when it comes in contact with the host medium and target. Consequently, the color of the solution changes (see Fig. 2C(d)). Therefore, micromotor-assisted colorimetric assays have laid the foundation for naked-eye detection. A schematic representation of all the mechanisms is shown in Fig. 2.

3. Micromotors for sensing of hazardous environmental pollutants

The advancements in technology, rapid industrialization, and various anthropogenic activities have brought a great threat to the water bodies, creating an alarming situation for both humans and aquatic creatures.[2,73] However, although many techniques are available for water monitoring and treatments, the world is still suffering from this threat due to the lack of superior and cutting-edge technology for the cost-effective, easy, and early detection of water pollutants to prevent water–borne diseases and save aquatic organisms. Hence, there is a great need for improved, faster detection of unwanted substances in water bodies to safeguard human and aquatic life.

During the last few decades, different micro/nanodevices have been widely employed for sensing poisonous environmental threats. All micro/nanomotors have been shown and proven as alternative tools in this field due to their unique properties such as rapid detection, very low detection volumes/concentrations, isolation of target molecules within a few minutes, and enhanced micro mixing.[74] In this regard, here, we discuss the role of micromotors in the detection of potential environmental pollutants such as various inorganic and organic substances.

3.1. Heavy metal ions

Heavy metal ions are the most active environmental hazards because of their toxicity, endurance in the environment, and bio-accumulative nature.[75] Various industrial, agricultural, and human activities have caused an increase in the content of these ions in the aquatic body, which severely affects the public health and aquatic creatures.[74,76,77] Although different spectroscopic techniques such as atomic absorption spectroscopy (AAS),[78,79] surface plasmon resonance spectroscopy,[80,81] inductively coupled plasma mass spectroscopy (ICP-MS),[82,83] electrothermal atomic absorption spectrometry,[84,85] and high-performance liquid chromatography (HPLC)[83,86] have been proposed to detect heavy metals in the water, there is still a lack of proper monitoring of these metals owing to the high cost, maintenance, and inadequacy of these techniques for *in situ* detection. Therefore, cost-effective and novel strategies are required for the early detection of these metals in the water body before it becomes catastrophic. Presently, the rapid progress in nanotechnology has given birth to synthetic micro/nanomotors, which hold considerable promise in this aspect in solving the current challenges by monitoring and detecting the pollutants by adopting various sensing mechanisms with the incorporation of different micro/nanomaterials.

As discussed in the previous section, fluorescence-based sensing has emerged as a suitable technique for the optical detection of molecules and analytes based on either the quenching or recovery of fluorescence signals. Jurado-Sanchez *et al.* first proposed the use of quantum dot-modified PEDOT/Pt tubular micromotors for the detection of mercury ions (Hg^{2+}).[87] The micromotors were prepared *via* the surface modification of positively charged poly diallyl dimethylammonium chloride (PDDA), which facilitated the attachment of the negatively charged CdTe quantum dots. Fig. 3A(a) shows a schematic and experimental representation of "on-the-fly" mercury ion detection *via* fluorescence quenching of CdTe. The inner Pt layer of the tubular microrocket causes self-propulsion by producing a bubble when treated with peroxide (H_2O_2) solution. The inset in Fig. 3A(a) represents an SEM image of the conical-shaped micromotors with an inner diameter of 2 μm and length of 18 μm. When the concentration of mercury ions was increased in the peroxide solution (kept at 5%), the intensity of the fluorescence signal decreased linearly up to 1 mg L^{-1} followed by rapid decay up to 3 mg L^{-1}, and at this point, complete quenching was noticed, as revealed in Fig. 3A(b). To test the selectivity and sensitivity of the micromotors towards mercury ions, the motile sensing probes were treated with some other ions (Cu^{2+}, Pb^{2+}, and CH_3Hg^+) in a large amount. However, no significant fluorescence quenching was observed in the presence of these ions, which revealed the efficient selectivity of micromotors towards mercury ions compared to other ions. Another interesting work using Pt-free Eu-MOF (metal organic framework)-based tubular micromotors towards the detection of Fe^{3+} ions was successfully reported by Yang *et al.*[57] In their work, interestingly, the tubular micromotors were fabricated using kapok fiber as a bio-template. Compared to other ions, the signal was quenched the most by Fe^{3+} ions, which shows the selectivity of the system. The MOF-based micromotors were obtained by the combination of hydrothermal treatment and various surface functionalizations. The schematic representation in Fig. 3B(a) highlights the constituents of the micromotor together with its quenching phenomenon upon the addition of Fe^{3+} ions. The micromotors swim in a medium following the catalytic decomposition of peroxide by MnO_2 nanoparticles (middle layer of micromotors). An event of the self-propulsion is shown in the inset of Fig. 3B(a). The presence of a hierarchically hollow structure and fluorescence phenomenon in the micromotors are owing to the innermost NiAl-CLDH (calcined layered double hydroxides) buffer layer and outermost Eu-MOF layer, respectively. It was shown that the emission peaks of the Eu-MOF-based motors, which were initially around the red region, were gradually nullified by the addition of Fe^{3+} ions successively. The intensity profile and inset in Fig. 3B(b) reveal the decrease in the emission peak height with an increment in ion concentration from 0 mM to 10 mM and the conversion from red color to dark, respectively. This shows the high sensitivity of micromotors toward detecting metal ions in water.

Fig. 3 Micromotors for heavy metal ion sensing. (A) (a) Schematic shows the "on-the-fly" detection of mercury ions by CdTe/PEDOT microtubes *via* fluorescence quenching and the real-time navigation of microrocket in 3 mg L^{-1} mercury solution. Inset: SEM image of rocket-like micromotor. (b) Graphical representation of fluorescence quenching (CCRF: calculated corrected total microsensor fluorescence) with an increment in mercury ion concentration in 5% peroxide solution, where inset shows the linear trend of fluorescence quenching phenomenon with respect to Hg^{2+} concentration. Reproduced with permission from ref. 87 Copyright 2015, The Royal Society of Chemistry. (B) (a) Fluorescence quenching of kapok-based Eu–MOF/EDTA (ethylenediaminetetraacetic acid)-NiAl-CLDH micromotor upon exposure to Fe^{3+} ions. Inset: Motion of micromotors due to catalytic decomposition of peroxide by MnO_2 nanoparticles. (b) Intensity profile depicts the variation in emission peak of fluorescence signal with an increase in the concentration of Fe^{3+} ions. Reproduced with permission from ref. 57 Copyright 2019, The Royal Society of Chemistry. (C) (a and b) Propulsion mechanism of PCL/Mg micromotor when encountered with silver ions and trajectory at different concentrations. (c) Speed of the eccentric Janus micromotor at different concentrations of Ag^+ ions. Reproduced with permission from ref. 54 Copyright 2019, Springer Nature.

Besides fluorescence sensing, inorganic metal pollutants have been detected *via* motion-based sensing. This type of mechanism relies on the speed of micromotors with reference to the concentration of the analytes. This strategy was first adopted by the Wang group in 2009.[88] They developed Au–Pt nanowires for the detection of metal ions. In the presence of silver ions, where the catalytic activities of both Au and Pt increased, which led to improved and faster movement of the motors. Alternatively, the catalytic activity of both metal segments decreased when attached to other metal ions. Similarly, this speed-enhancement property of silver ions was also shown

later by Zhang *et al.*, who fabricated bubble-propelled eccentric PCL/Mg Janus micromotors of approximately 50 μm diameter through a one-step emulsion method.[54] When these motors were placed in a 3 wt% H_2O_2 solution, no motion was observed. However, interestingly, the micromotors moved by forming oxygen bubbles when encountering silver ions, as shown in Fig. 3C(a). The attachment of silver ions on the surface of the Mg sphere is due to the displacement reaction, which results in propulsion *via* the formation of an oxygen bubble on the surface of the motors. The trajectory and speed of the micromotors were studied for silver–ion treated peroxide solution. An

increasing concentration of silver ions at a fixed concentration of peroxide created spiral tracks, as shown in Fig. 3C(b). The spiral movement of motors is attributed to the resultant propulsive force acting away from the center of mass. Hence, this unequal distribution of forces at different parts of the motors pushes them both in a translational and rotational manner, which is ultimately reflected in the form of spiral tracks. In addition, the speed of the motors increased with an increase in the concentration of ions due the occurrence of a rapid displacement reaction, as depicted in Fig. 3C(c). Other precious metal ions such as Pt^{2+}, Pd^{2+}, and Au^{2+} were employed to test the sensitivity of motors. When the micromotors were treated with these noble metal ions for 5 min, the motors showed fair propulsion speed. On the contrary, when the treatment time was shortened to 5 s instead of 5 min, no propulsion was observed. However, when the motors were fortified with a silver ion-containing solution, they showed rapid propulsion within 5 s of treatment, which shows the greater sensitivity of the micromotors towards silver ions compared to other ions.

3.2. Chemical warfare agents and explosives

The rapid surge of chemical warfare agents (CWA) and explosives through terrorist assaults and other activities have posed a serious threat to human health in recent years.[59,89] Accordingly, researchers have devoted their efforts to developing novel approaches for the rapid detection of these types of mass destructive weapons to safeguard life. Consequently, different methodologies such as mass spectrometry,[90] Raman spectroscopy,[91] ion mobility spectrometry,[92] interferometry,[93] chromatography,[89] electrochemical assays,[94] and fluorescence polarization,[62,95] have been proposed and used. However, the application of these techniques for real-time detection and monitoring is limited by their complex operation, low sensitivity, and inaccurate data production.[96] Thus, fast and reliable sensing techniques are urgently needed to encourage their timely detection. In this case, the current trends and advancements in micro/nanomotors have shown the potential to address the above-mentioned problems and proven versatility in human security by coupling their self-propulsion with the functionality of the detection mechanism.

Nerve agents are one of the most fatal CWAs, possess enough toxicity to disrupt the mechanism of neurotransmissions, which leads to severe health problems such as cardiac arrest, unconsciousness, and sometimes even death.[96] The fluorescence "ON–OFF"-based screening strategy was first adopted by Singh et al. for the detection of sarin and soman, which are considered nerve agents.[68] The dye-coated silica-Pt Janus micromotors exhibited fluorescence quenching upon exposure to sarin and soman. The mechanism of quenching can be understood based on Fig. 4A(a), where the fluorescence property is interrupted due to the release of HCl, which causes inhibition of the conjugation of the fluorophore in the diethyl chlorophosphate (DCP) and fluoresceinamine (FLA) phosphoramidation reaction. The as-prepared FLA-coated self-propelled micromotors showed quick quenching of the fluorescence signal upon exposure to DCP within a few seconds compared

to their static counterparts (Fig. 4A(b)). Moreover, the sensing efficacy of the micromotors was investigated by varying the concentration of DCP. Fig. 4A(c) highlights the time-dependent quenching phenomenon at different concentrations of DCP, ranging from 10^{-1} to 10^{-6} M. The quenching effect of the micromotors was observed to be extremely fast for more than 10^{-3} M DCP within a minute and the detection limit was found to be in the order of 10^{-6} M. Besides nerve agents, some natural toxins are considered to be lethal owing to their ability to incapacitate cellular functions. Ricin is a poisonous chemical agent, which is extracted from the castor plant. Given that it consists of two polypeptide chains, it suppresses the synthesis of protein at the cellular level and leads to the death of cells. The group of J. Wang first demonstrated a fluorescent "OFF–ON" micromotor platform for the ricin detection at extremely low concentrations.[36] The fluorescein-amidine (FAM) dye-coated reduced graphene-oxide(rGO)/platinum (Pt) tubular micromotors were tagged with ricin B aptamer to selectively sense the target ricin B in the solution. The graphene surface of the micromotors induced the quenching effect due to the π–π interactions between the surface of the carbon material and nucleotide bases of the FAM dye. An increase in the fluorescence signal in the dye-coated aptamer was observed when it was released in a peroxide medium mixed with the target ricin B. The recovery of the signal is attributed to the strong affinity between the aptamer and target compared to the GO surface. Fig. 4B(a) displays the fluorescence "OFF–ON" events in the presence of GO/Pt micro engines, peroxide, receptor, and target toxins. The correlation between the concentration of target ricin B and the fluorescence signal was established and observed from the calibration plot, as shown in Fig. 4B(b). The linear increment in the signal from 0.1 ng mL^{-1} to 10 000 ng mL^{-1} concentration of the target depicts the attractive and strong interaction between the aptamers and targets, which indicates the greater sensitivity of the motile micromotors towards the ricin B toxin. The tubular morphology of the micromotors was confirmed from the scanning electron microscopy (SEM) image, as shown in the inset. The hazardous impact of devastating explosives on living entities has been a significant issue in this arena. According to the United States Environmental Protection Agency (USEPA), nitroaromatic explosives such as TNT have been found to have both mutagenic and cancer-causing effects on human health. In this regard, Yuan et al. designed up-conversion nanoparticle (UCNP)-modified spherical Janus micromotors for the rapid detection of TNT to strengthen the security of human beings as well as environments.[59] The schematic in Fig. 4C(a) represents the fluorescence "ON–OFF" detection mechanism of TNT by Janus micromotors. To show the quenching effect, the UCNPs were functionalized with poly(acrylic acid) (PAA), followed by 3-aminopropyltriethoxysilane (APTES). The amino groups of UCNPs create a Meisenheimer complex by interacting with TNT. The reduction in luminescence intensity of the micromotors upon exposure to TNT was explained based on the fluorescence resonance energy transfer (FRET) mechanism. Given that the emission spectra of the excited UCNPs coincide with the absorption spectra of the as-obtained Meisenheimer

Fig. 4 Chemical warfare agent and explosive detection. (A) (a) Schematic representation of the dye-coated silica-Pt Janus micromotors for the "ON–OFF" detection of sarin and soman and the chemical reaction involved during the fluorescence quenching phenomenon. (b) Decay of fluorescence signal of micromotors in real-time upon exposure to DCP and comparative plot representing the rapid decrease in the intensity as compared to the static counterpart. (c) Fluorescence count variation as a function of time and concentration of DCP. Reproduced with permission from ref. 68 Copyright 2015, The Royal Society of Chemistry. (B) (a and b) "OFF–ON" fluorescence sensing of ricin-B toxin by dye-ricin B aptamer-functionalized GO/Pt micromotors and the interrelationship between fluorescence intensity and concentration of target ricin B. Inset: SEM image of conical microstructure. Reproduced with permission from ref. 36 Copyright 2016, the American Chemical Society. This is an open access article distributed under an ACS Author Choice License. (C) (a) Schematic highlighting the fluorescence quenching of UCNP-modified spherical Janus motor due to the detection of an explosive (TNT). Real-time event of fluorescence intensity variation without TNT (b) and with 0.5 mg mL^{-1} TNT (c) in 5% peroxide solution was captured for 5 s and 9 s, respectively. Reproduced with permission from ref. 59 Copyright 2019, Beilstein Journal of Nanotechnology. This is an open access article distributed under the terms of the Creative Commons Attribution License.

complex, this resulted in a reduction in the intensity of the luminescence signal. To show the sensitivity of the motors towards TNT, two experiments were carried out in peroxide solution, *i.e.*, one without TNT and the other with TNT. There was no significant change in the intensity of the emission spectra of the UCNP-modified micromotors in TNT-deficit medium in 5 s, whereas the TNT-rich medium showed a drastic decay in intensity within 9 s (Fig. 4C(b and c)). Thus, UCNP-functionalized Janus micromotors can act as active sensors for the accurate screening of TNT with a good limit of detection (LOD: 2.4 ng mL^{-1}). The same year witnessed the fluorescence detection of another powerful

nitroaromatic explosive, *i.e.*, TNP (2,4,6-trinitrophenol) by Wang *et al.* with the help of self-propelled covalent-organic-framework (COF)-based micromotors.[97] The incorporation of Fe$_3$O$_4$ nanoparticles and MnO$_2$ microparticles in the biodegradable polycaprolactone (PCL) microspheres facilitated the guided autonomous motion of micromotors. The Py-azine COF helped in the detection of TNP in aqueous media by exhibiting the fluorescence quenching phenomenon. The rapid quenching effect is attributed to the interaction of azine with TNP through the formation of hydrogen bonds and enhanced fluid mixing enables the faster sensitivity of the COF-based micromotors towards this explosive compound.

3.3. Gases and other pollutants

Different types of harmful gases such as ammonia, hydrochloric acid, and some other organic pollutants are released into the water environment because of natural disasters such as volcanic eruptions and man-made activities mainly in the agricultural, industrial, and pharmaceutical fields.[98] This has led to a myriad of hazardous impacts on water living species and humans in many ways. Being highly soluble in water, these gases and pollutants change the pH of water bodies and unprecedentedly cause damage to the aquatic ecosystem and humans *via* the bioaccumulation process. Thus, long-term exposure to these materials causes skin diseases, respiratory problems, stomach inflammation, *etc.* Among the different proposed techniques, the self-acting micromotors have set a paradigm in the field of sensing to probe pollutant analytes from the solution.

For instance, the ability of micromotors as a gas sensing platform was first demonstrated by Dong *et al.* using iridium-gold-based Janus microspheres to detect hydrazine vapor from the surrounding atmosphere.[99] Later, Liu *et al.* constructed metal-free noncorrosive hexagonal-shaped micromotors for the detection of HCl and NH$_3$ gas molecules with good precision and low detection limit.[58] They reported the preparation of a biodegradable polycaprolactone (PCL) and catalase (CAT)-based fluorescent micromotor, which has the capacity to generate bubbles during propulsion in hydrogen peroxide solution and identify toxic gas molecules based on the change in their fluorescence signal. The variation in signal intensity is attributed to the characteristics of fluorescein isothiocyanate (FITC) dye molecules. This dye exhibits different forms when exposed to an acidic and basic environment, *i.e.*, in HCl medium, it shows an extremely weak and faint signal due to its non-fluorescent neutral form, whereas ammonia medium results in a stronger peak on account of the formation of a dianion structure. The described phenomenon of consecutive detection of both HCl and NH$_3$ gas by the CAT-PCL-FITC micromotor is highlighted in Fig. 5A. Fig. 5A(a) presents a schematic representation of the detection of these toxic gases by the motile

Fig. 5 Detection of gases and other pollutants by micromotors. (A) (a) Schematic diagram of the sensing of hydrogen chloride (HCl) and ammonia (NH$_3$) gases by CAT-PCL-FITC micromotor. (b–g) Disappearance and reappearance of fluorescence signal upon exposure to HCl gas (4 s to 5 s) and NH$_3$ gas (5 s to 7 s) in a consecutive manner. Reproduced with permission from ref. 58 Copyright 2016, The Royal Society of Chemistry. (B) Schematic illustration of the synthesis of HRP-MIL-100(Fe)@TiO$_2$@Fe$_3$O$_4$ micromotor and its assistance in the colorimetric detection of hydroquinone. MIL: Materials of Institute Lavoisier. Reproduced with permission from ref. 69 Copyright 2022, the American Chemical Society.

micromotors due to the change in their signal intensity upon continuous exposure to 488 nm light and the real captured event is highlighted in Fig. 5A(b–g). When 9000 ppm HCl gas was passed through the micromotor-rich solution, the signal gradually faded and at 5 s it was almost gone (see Fig. 5A(b–e)). Alternatively, when the same amount of NH_3 gas was applied, subsequently the fluorescence signal recovered, and hence the motors reappeared (Fig. 5A(f and g)). Thus, these gas sensing micromotors can be a potential probing tool for environmental monitoring.

Besides fluorescent-dependent detection mechanisms, colorimetric detection has gained significant attention due to its high efficiency and feasibility by obviating the necessity of sophisticated and costly instruments. This cost-effective technique was used by Yang et al. to detect hydroquinone (HQ) by using 3,3′,5,5′-tetramethylbenzidine (TMB) with the three-dimensional (3D) multifunctional Janus micromotors.[69] The 3D structure was prepared via the layer-by-layer (LBL) self-assembly method, as shown in Fig. 5B. The schematic shows the process starting from their synthesis to the colori-

metric detection of HQ, which is comprised of 4 steps. The first 3 steps involve the formation of a horseradish peroxidase (HRP)-immobilized patterned and flower-shaped multifunctional Janus microstructure via hydrothermal and coprecipitation methods. The final step reveals the mechanism of the colorimetric detection of HQ. The dual oxidase and peroxidase-like properties of the Janus motors produce $^\bullet OH$ and $^\bullet O_2^-$ by catalyzing oxygen and peroxide molecules, respectively, which change the color of TMB to blue color via oxidation. When HQ was added to the solution, oxTMB is reconverted to TMB with p-benzoquinone (Bq) tautomer due to the strong reducibility of HQ. Hence, the whole reaction made the solution colorless again. This type of unique, novel, and smart platform dynamically sensed HQ with a LOD 1.84 μM, which can pave the way toward the environmental protection field.

All the recent significant works on the detection of hazardous environmental pollutants such as heavy metal ions, CWA, explosives, gases, and other pollutants are summarized in Table 1.

Table 1 Micromotors for the detection of hazardous environmental pollutants

Name of micro/nano-motors with size	Materials	Target	Sensing mechanism	Author (year)
Heavy metal ions				
Tubular and 8 μm length	PEDOT/Au-catalase	Hg^{2+}, Cu^{2+}	Motion-based (speed reduction)	Orozco et al.[100] (2013)
Tubular	Cu/Pt bimetallic	Pb^{2+}	Motion-based (speed reduction)	Moo et al.[101] (2014)
Tubular and 18 μm length	CdTe/PEDOT	Hg^{2+}	Fluorescence quenching	Jurado-Sánchez et al.[87] (2015)
Tubular and 12 μm length	ZnS-polyaniline (PANI)-Pt	Hg^{2+}	Fluorescence quenching	Jurado-Sánchez et al.[102] (2016)
Tubular and 67 ± 14 μm length	g-C_3N_4 (GCN)	Cu^{2+}	Fluorescence quenching	Villa et al.[103] (2018)
Tubular and 700 nm length	Pt–Halloysite	Hg^{2+}	Motion-based (speed reduction)	Maric et al.[104] (2019)
Tubular and 108.8 μm length	Eu-MOF/EDTA-NiAl-CLDH	Fe^{3+}	Fluorescence quenching	Yang et al.[57] (2019)
Eccentric Janus and 50 μm diameter	PCL/Mg	Noble metal ions (Pt^{2+}, Pd^{2+}, Au^{3+}, Ag^+)	Displacement reaction (speed enhancement)	Zhang et al.[54] (2019)
Tubular	AO–Mn_2O_3/γ-AlO (OH)	Hg^{2+}	Fluorescence quenching	Li et al.[105] (2021)
Tubular	BSA-$NiCo_2O_4$@MnO_2/C	Cu^{2+}	Colorimetric sensing	Yang et al.[106] (2021)
Chemical warfare agents (CWA) and explosives				
Janus sphere and 45 μm diameter	FLA/silica-NH_2/Pt	Sarin and soman (DPP)	Fluorescence quenching	V. Singh et al.[68] (2015)
Janus sphere	Mg/Au	Paraoxon	Electrochemical sensing	Cinti et al.[107] (2015)
Tubular and ∼6 μm length	PEDOT/Au	Diethyl chlorophosphate (DCP)	Motion-based (speed reduction)	V. Singh et al.[108] (2016)
Tubular and ∼10 μm long	reduced graphene-oxide (rGO)/platinum (Pt)	Ricin	"OFF–ON" fluorescence detection	Esteban-Fernandez de A Vila et al.[36] (2016)
Spherical and 30–40 μm diameter	COF (covalent organic framework)	Trinitrophenol (TNP)	Fluorescence quenching	Wang et al.[97] (2019)
Spherical and 5 μm diameter	UCNP capsule motors	TNT (2,4,6-trinitrotoluene)	Fluorescence quenching	Yuan et al.[59] (2019)
Tubular and 100 μm length	COF-functionalized Pt motors	2,4,6-Trinitrophenol	Fluorescence quenching	Wang et al.[66] (2021)
Gases and other pollutants				
Hexagonal and 10 μm length	CAT-PCL-FITC (catalase-polycaprolactone-fluorescein isothiocyanate)	HCl and NH_3 gases	Fluorescence quenching	Liu et al.[58] (2016)
Spherical and 20 μm diameter	Mg/Au	DPP (diphenyl phthalate)	Electrochemical sensing	Rojas et al.[109] (2016)
Tubular and ∼12 μm length	Single Wall (SW)−Fe_2O_3/MnO_2	Phenylenediamine isomers	Colorimetric sensing	María-Hormigos et al.[110] (2018)
Spherical and 0.6 μm diameter	HRP-MIL@TiO_2-MMT	Hydroquinone (HQ)	Colorimetric sensing	Yang et al.[69] (2022)

4. Micromotors in the process of biosensing

The current progress in analytical biosensing is significant in the field of biomedical diagnosis and treatment.[111] Many techniques such as enzyme-linked immunosorbent assays (ELISA),[112–114] surface-enhanced Raman scattering (SERS),[115,116] polymerase chain reaction (PCR),[117–120] and various optical sensing tools[72] have been widely exploited for the detection of micropathogens, biomolecules, biomarkers, and infectious target cells. However, these methods require complex operation steps and a long analysis period for the detection of the targets. Accordingly, the emergence of micro/nanomotors has opened a new avenue and promoted reliable, fast, and non-cumbersome detection methods for investigating and analyzing biological analytes by adopting optical, electrochemical, and motion-based sensing mechanisms.[16] Mainly, the working principle of these motile micro/nano motor-based biological sensors depends on the interaction of the bioreceptor unit with the target bioanalytes.

4.1. Micropathogens and cells

Micropathogens (bacteria, viruses, and fungi) are organisms that pose a threat to humans and other living species.[122] They are the cause of various contagious diseases. Thus, the quick and selective detection of these biological contamination species is of great value for food safety, medicine, and environmental monitoring. The strategy to identify the presence of bacteria and fungi in a medium is based on either their direct detection or via toxin detection, which is produced from their body. Most of the methods confirm their presence based on the detection of the toxic substances released from their body. Additionally, the growth of infectious and lethal tumor cells in humans is becoming more devastating, resulting in the death of many patients.[123] Thus, it is an urgent requirement to timely detect these fatal cells before they mutate and proliferate and affect the whole body. The survival of the patient, reoccurrence, and propagation of these cancerous cells are decided based on their detection stage and accurate determination of their quantity. Hence, the researchers are focusing on the utilization of auto-propelled micromotors for the rapid sensing of these micro-organisms and cells due to their novel properties.

Endotoxins or lipopolysaccharides (LPSs) are present in the outer membrane of Gram-negative bacteria and have a severe impact on the immune system of the human body when released into the bloodstream. Thus, the idea of detecting these toxic compounds by micromotors was first conceptualized and demonstrated by the group of Alberto Escarpa. In their study, they proposed the use of a graphene quantum dot-modified Janus micromotor for the detection of LPS.[124] The emulsion method was adopted to develop a magneto-catalytic Janus structure, where Pt, Fe_3O_4 nanoparticles and phenylboronic acid (PABA)-modified graphene dots were embedded in PCL (polycaprolactone) microspheres. The fast-moving structure with a highly specific recognition unit enabled the ultrafast detection of endotoxins. The interaction between the endotoxin molecules and PABA caused the fluorescence quenching of the

quantum dots and the LOD was found to be 0.01 M. A similar type of strategy was later adopted for the detection of *Salmonella enterica* in food samples such as egg and milk. However, the selectivity of PABA was very poor to detect different types of endotoxins given that keto-deoxyoctulosonate (KDO) residue is common in most bacteria. Also, the time and limit of detection of the sample were not satisfactory, *i.e.*, not relevant for clinical sample analysis. Thus, to solve these problems, the same group developed a new type of micromotor with higher selectivity and sensitivity. The modified micromotor consisted of 2D WS_2 nanomaterials for selective binding with a rhodamine-labeled affinity peptide, which senses the *Escherichia coli* O111:B4 lipopolysaccharide (LPS) from the biological sample with a LOD of 120 pM.[56] The quenching-recovery activity is shown in Fig. 6A. When the micromotors were added to the solution of affinity peptide, they interacted with WS_2 and got stuck, thus losing their fluorescence property. Subsequently, their fluorescence property was regained on interacting with the endotoxins when added to the solution. This robust and selective platform with a low detection ability indicates the tremendous capability of micromotors for the analysis of real clinical samples.

In addition to bacterial endotoxin contamination, fungus-induced toxins, *i.e.*, mycotoxins, are mainly responsible for many acute to severe diseases. Generally, mycotoxins are found in foodstuff, indicating the presence of mold or fungus in the sample. Thus, the precise detection of mycotoxins in food samples has a great importance in food-quality monitoring. The group of Alberto Escarpa pioneered a graphene-based tubular micromotor strategy for the analytical sensing of mycotoxins in a Certified Reference Material (CRM) and complex food samples.[121] To demonstrate the performance of the reduced graphene oxide (rGO)/Pt micromotors, two harmful mycotoxins, *i.e.*, fumonisin B1 (FB1) and ochratoxin A (OTA), were employed. Fig. 6B presents the "OFF–ON" fluorescence strategy of the motile microtubes towards these mycotoxins. The interaction between the ring-like structures of the nucleotide bases of the aptamer and hexagonal cells of the graphene surface led to the quenching of the fluorescent signal of the fluorophore-modified aptamers. When mycotoxins were added to the solution, the affinity between specific aptamers and mycotoxins became strong, which resulted in the recovery of the fluorescence signal in the solution. This new approach demonstrated the highly sensitive detection of mycotoxins with a LOD of 7 and 0.4 ng mL^{-1} for OTA and FB1, respectively, within 2 min for 1 μL sample. This new mycotoxin sensing strategy expands the possibility and horizons of the field of micromotors for food safety diagnosis in the near future.

Besides bacterial and fungal threats, viruses are another potent devasting biological infectious agent, which can cause quick death when bound to the cells of a body. The Zika virus is one of the viruses that has become a global health concern because of its potency in inducing neurological complications. According to the literature, during the Zika virus outbreak, the world witnessed an increase in Guillain−Barre syndrome and microcephaly in newborn babies.[125] However, to date, there is no medication or vaccine for this virus. Thus, to safeguard the

Fig. 6   Micromotors for the sensing of micropathogens and cells. (A) Schematic and fluorescence microscopy image of affinity peptide-modified WS$_2$-based micromotor for fluorescence ''OFF−ON'' detection of *Escherichia Coli* endotoxin. Reproduced with permission from ref. 56 Copyright 2020, Elsevier. (B) Utilization of unmodified rGO/PtNP micromotors for mycotoxin detection. Top part shows the fluorescence quenching event of the solution in the absence of mycotoxin because of the affinity between the ring-like structures of nucleotide bases of aptamer and hexagonal cells of graphene surface, whereas the bottom part throws light on the recovery of the signal in the mycotoxin-added solution due to the specific interaction between aptamer and mycotoxins. Reproduced with permission from ref. 121 Copyright 2017, the American Chemical Society. (C) (a) Schematic of cell phone-based system for the detection of Zika virus assisted by Pt nanomotors. (b) Concentration-dependent speed (see plot) and trajectory of nanomotor-based bead in the control experiment and virus-loaded sample with varying concentrations. Reproduced with permission from ref. 37 Copyright 2018, the American Chemical Society. (D) (a) Schematic illustration of motion-capture-ratiometric fluorescence sensing of circulating tumor cells (HepG2 cells) by TLS11a aptamer-conjugated Janus rods. (b) Plot indicates the ratiometric fluorescence response (simultaneous decrement and increment in emission peak for TPE-T at 450 nm and FITC-G at 526 nm, respectively) at varying concentrations of target tumor cells. Reproduced with permission from ref. 64 Copyright 2019, Elsevier.

life of infants and to avoid the severity of the viral infection in common people, there is a huge demand for the early-stage detection and diagnosis of this virus. Draz *et al.* adopted the motion-based sensing strategy for the detection of Zika virus using Pt nanomotors.[37] Fig. 6C(a) illustrates the nanomotor-based bead-motion cell phone (NBC) system for the virus detection in peroxide medium. Specifically, 3 μm PS beads were attached with the monoclonal antibody (anti-ZIKV mAb) to capture the Zika virus. Similarly, the anti-ZIKV mAb was used to modify Pt nanoparticles. When the Zika virus-containing beads were mixed with the modified Pt nanoparticles in the peroxide solution, the motile nanoparticles were attracted to the Zika virus beads and improved their rate of propulsion. The

whole scenario and analysis of the speed of the PS beads were done in the NBC system. The concentration-dependent speed of the micromotors and their trajectory were also studied using the NBC system, as shown in Fig. 6C(b). A change in the velocity of the PS beads was observed with the addition of varying concentrations of Zika virus. Upon the addition of the virus in increasing order ranging from 10^0 particles μL^{-1} to 10^6 particles μL^{-1}, the antibody-modified Pt quickly bonded with the Zika virus-loaded PS beads, resulting in their vigorous motion. To test the specificity and efficacy of the motors towards the detection of Zika virus, the peroxide solution medium was fortified with Zika virus sample together with some other viruses (dengue virus, herpes simplex virus type 1, and human

cytomegalovirus). This NBC system offered specific detection together with the quantitative measurement of a Zika virus-loaded sample with a low limit of detection (1 particle μL^{-1}). In the same year, Draz *et al.* illustrated the use of DNA-engineered micromotors for the detection of HIV-1 by utilizing a cell phone system.[126] The integration of loop-mediated isothermal DNA amplification, Pt, and Au nanoparticle-functionalized PS bead-based micromotors and a cell phone system allowed the quantitative detection of HIV-1 (n = 54) at a clinically relevant threshold value of 1000 virus particles mL^{-1} with high sensitivity and selectivity.

Cancer metastasis is becoming a major concern owing to its fatality nowadays.[127] It is basically the migration of tumor cells from one area to another area in the body. Therefore, it is highly important to detect circulating tumor cells (CTC) to know the status of tumor cell propagation and growth for the early diagnosis and treatment of a patient.[63,128] However, given that the CTC concentration in the blood is extremely low, its selective identification in the presence of a large number of hematological cells is a great challenge. Thus, Zhao *et al.* adopted low-cost technology to fabricate fibrous Janus rods for the sensing of CTC (human liver tumor cells HepG2) through the ratiometric fluorescence detection strategy.[64] The fabricated Janus rods (electrospinning and cryocutting methods) contained two surfaces, *i.e.*, one was modified with catalase for propulsion, whereas the other was functionalized with TLS11a aptamers, thymine-conjugated tetraphenylethene (TPE), and guanine-conjugated fluorescein isothiocyanate (FITC) for ratiometric fluorescence signal generation when capturing the target cells. The aggregation-induced emission (AIE) and aggregation-caused quenching (ACQ) effect induced the generation of a blue signal and inhibited the green signal of TPE and FITC, respectively, in the initial phase. When the tumor cells were captured by the rods, then TPE and FITC were released from the body of the Janus rods, which resulted in the green signal emission of FITC and suppression of the blue signal of TPE (Fig. 6D(a)). They also demonstrated the quantitative detection of tumor cells together with their ratiometric intensity profile with varying concentrations, as shown in Fig. 6D(b). The intensity plot shows how the increasing trend in the concentration of tumor cells affects the ratiometric signal generation. With an increase in the concentration of cells, the emission spectra of TPE-T at 450 nm and FITC-G at 526 nm decreased and increased, respectively. The continuous solution mixing provided by the self-propelled micromotors enhanced the CTC capture and generation of the ratiometric signal, which promoted the low detection limit (25 cells mL^{-1} in blood within a minute) and rapid sensing. This easy method allows naked-eye visualization for the sensitive detection of the cells in an economical way.

The works reported by various research groups towards the detection of micropathogens and cells are summarized in Table 2.

4.2. Biomolecules

Biomolecules are the fundamental chemical basis of all living organisms. They are broadly classified into proteins, carbohydrates, nucleic acids, and lipids. The structure and function of all cells depend on the concentration of these molecules. Any variation in the amount of biomolecules in the body results in the non-functionality of cells and abnormality in the behavior of organisms. Therefore, these biomolecules are indicative parameters or biomarkers of different types of diseases.[136] Mostly these biomarkers are found in body fluids such as blood, urine, and tissues and are potent tools for the identification and treatment of many life-threatening diseases. Hence, the precise detection of these biomolecules is necessary for protecting our bodies from various diseases. Artificial self-propelled micromotors have been successfully employed for the accurate and expeditious detection of these biomarkers owing to their multi-functional structural body-like sensing and propulsion unit. In this context, we first discuss the detection of some biomolecules by micromotors, and secondly, we highlight the biomarker sensing and their roles in the detection of biomolecules.

Deoxyribonucleic acid (DNA) is a special type of biomolecule that possesses the genetic information responsible for the growth and development of an organism. If any damage occurs to it, it can induce genetic disorders and many diseases in organisms. Thus, DNA sensing has been a hot area in recent years in the biomedical field. Based on this, the team of Wang first reported a motion-based biosensor for the sensitive detection of DNA.[38] This method relied on bimetallic nanowires (Au–Pt) for sensing the target DNA in the presence of silver ion -enriched peroxide medium. In their experiment, the nanomotor motion was enhanced by silver ions. It should be noted that here, the nanomotor propulsion and sensing showed a strong dependency on the ionic strength of the medium. This indicates that the sensing ability not only depends on the target analyte, but it may also be affected by the concentration of the ions (silver). Considering this, we can conclude that this type of nano-sensing probe may suffer from inefficient sensitivity and specificity. Later, an enzyme-powered micromotor was proposed by Ju and co-workers, in which poly(3,4-ethylenedioxythiophene and sodium 4-styrenesulfonate)/Au microtubes (PEDOT-PSS/Au) were fabricated *via* the electrodeposition method, which produced the motion-based signal only in the presence of the target DNA without maintaining any specific concentration of sensing probes. Here, both the sensing and power units were incorporated in one layer, and thus when the target DNA contacted the sensing unit, it would directly reduce the motion of the micromotors by affecting the power unit.[138] This catalase-modified micromotor showed better efficacy towards specific target sensing. However, although it solved the problems of the detection of specific DNA targets, it still faced the challenge to get a higher surface area for accommodating more sensing and power units due to its micro-space tubular morphology. Considering all the practical challenges, the group of Ju later fabricated jellyfish-like micromotors to realize a higher inner surface area for the accommodation of the biosensing unit and power unit.[55] Fig. 7A(a) shows the layer-by-layer morphology of the metallic shell decorated with DNA assembly (sensing unit) and catalase-modified assembly (power unit). The DNA assembly followed a sandwich-like hybridization (DNA1/2/3) on the concave surface of gold. When the target DNA came in contact with the shell, DNA 2 hybridized with the target DNA,

Table 2 Micropathogen and cell detection

Name of micro/nano-motors with size	Materials	Target	Sensing mechanism	Limit of detection	Author (year)
Bacteria					
Tubular and 18 µm length	MIP (magnetically imprinted)–PEDOT/PSS	Phycocyanin (cyano-bacterial bloom)	Fluorescence detection	—	Zhang et al.[129] (2015)
Spherical and 20 µm diameter	Magneto catalytic Graphene Quantum Dots	LPS 0111:B4 (Escherichia coli bacteria)	Fluorescence quenching	0.01 M	Jurado-Sa'nchez et al.[124] (2017)
Spherical and 20 µm diameter	PtNPs and Graphene QD-modified microsphere	Lipopolysaccharides (Salmonella enterica)	Fluorescence quenching	0.07 ng mL^{-1}	Pacheco et al.[130] (2018)
Janus rod-1 (5 µm length), JR-2 (10.5 µm), JR-4 (19.8 µm)	PSMA-PEI-CAT/PSMA-TPEC-Man	E. coli bacteria	Fluorescence detection (change in color of signal)	45 CFU mL^{-1}	Zhao et al.[131] (2019)
Tubular and ∼12 µm length	WS$_2$/Pt and MoS$_2$/Pt	0111:B4 endotoxins (Escherichia coli)	Fluorescence recovery	1.9 ng mL^{-1}	Víctor de la Asuncion-Nadal et al.[132] (2020)
Spherical Janus	WS$_2$–Pt–Fe$_2$O$_3$ polycaprolactone	O111:B4 LPS (Escherichia coli)	Fluorescence recovery	120 pM	Pacheco et al.[56] (2020)
Spherical Janus	Graphdiyne oxide (GDYO)-, black phosphorous (BP)-, or graphene oxide (GO)-wrapped Janus micromotors	Cholera toxin B (Vibrio cholera)	Fluorescence recovery	0.002, 0.003, and 0.015 µg mL^{-1} for GDYO, GO, and BP motors, respectively	Yuan et al.[133] (2020)
Spherical Janus and <10 µm diameter	WS$_2$/MoS$_2$	Typhimurium endo-toxin (Salmonella enterica)	Fluorescence recovery	1.2 µg mL^{-1}	Pacheco et al.[134] (2022)
Viruses					
Spherical and ∼4.4 nm diameter	Pt nanomotors	Zika virus	Motion-based detection (speed enhancement)	—	Shehata Draz et al.[37] (2018)
Spherical and 6 µm diameter	Au and Pt NP-DNA-modified PS beads	HIV-1 Virus	Motion-based detection (speed reduction)	1000 virus particles mL^{-1}	Shehata Draz et al.[126] (2018)
Fungi and cells					
Tubular and ∼10 µm length	rGO/PtNPs	Mycotoxins, e.g., OTA and FB1 (fungus)	Fluorescence recovery	7 and 0.4 ng mL^{-1} for OTA and FB1	Molinero-Fernandez et al.[121] (2017)
Tubular	Magnetic rGO/Ni/PtNPs micromotors	Mycotoxins, e.g., OTA and FB1 (fungus)	Fluorescence recovery	0.0007 and 0.004 µg mL^{-1} for FB1 and OTA	Molinero-Fernandez et al.[135] (2018)
Janus rod-0.4 (1.9 µm length), JR-1 (4.9 µm), JR-2 (10.4 µm), and JR-4 (19.8 µm)	Aptamer (TLS11 a) and catalase modified rod	Circulating tumor cells (Hep G2)	Ratiometric fluorescence detection	25 cells mL^{-1}	Zhao et al.[64] (2020)

resulting in the release of the catalytic catalase unit from the structure. This reduced the speed of the micromotors. A decreasing linear trend in the speed of the micromotors was observed due to the addition of more target DNA in the peroxide solution (Fig. 7A(b)). Owing to their biocompatible nature and larger inner opening, these micromotors showed potential in the fast and reliable motion-based sensing of DNA in a protein-rich biomedium.

Proteins are the essential nutrients of the body and are considered as building blocks with multifunctional behaviors. They play a significant role in the metabolic activity of the body such as repairing tissues, maintaining a balanced energy level and the production of antibodies. Thus, the detection of proteins has become necessary to understand cellular functions, clinical diagnosis, and treatments. In this case, self-propelled tags were first demonstrated for protein detection with no requirement for the polymerase chain reaction (PCR) method.[137] This strategy involved the electrochemical detection of protein by movable tubular IrO$_2$/Pt micromotors. Fig. 7B(a–c) show a schematic representation of the steps involved, from the fabrication of the microtubes to the electrochemical detection

of the protein (rabbit IgG). Here, the inner platinum layer served as the propulsion layer and the outer metal oxide (IrO$_2$) as the electroactive label (help in protein detection by hydrogen evolution reaction). The fabricated microtubules (via electrodeposition) were conjugated with antirabbit IgG, and in parallel the tosyl-activated magnetic beads (MBs) were functionalized with antirabbit IgG for the magneto-immunoassay. Both the MBs and tags were incubated with rabbit IgG in a mixed solution of 0.8 wt% H$_2$O$_2$, 1 wt% of SDS, and a buffer of pH 7.4 to get the actuation and selective detection of the protein via magneto-immunoassay. Ultimately, the hydrogen evolution reaction resulted in the protein detection in the presence of 0.5 M H$_2$SO$_4$. The autonomous motion of the microtubes and incorporation of magneto-immunoassay improved the fluid mixing and enabled the quick, selective, and sensitive detection of the target protein within a few minutes. The micromotor-assisted electrochemical detection of protein was observed using the chronoamperometry technique.

Further, we provide insight into the detection of biomolecules via the identification of biomarkers. In the detection of biomarkers, a new approach was reported for the

Fig. 7 Schematic representation of DNA and protein biomolecule sensing. (A) (a) Schematic illustration of jellyfish-like micromotor decorated with sensing unit (DNA1/2/3) and power unit (S1/S2 assembly with catalase) on the concave Au surface. Inset: SEM image. (b) DNA sensing of micromotor via speed reduction mechanism and the corresponding plot shows the correlation between the speed of the motors and concentration of target DNA. Reproduced with permission from ref. 55 Copyright 2019, the American Chemical Society. (B) (a) Fabrication of IrO₂/Pt microtubes via template-assisted electrodeposition. (b) Surface functionalization with antibody for the preparation of a magneto-immunosandwich assay. (c) Electrochemical detection of protein (rabbit IgG) through hydrogen evolution reaction (HER) catalysis. Reproduced with permission from ref. 137 Copyright 2019, John Wiley and Sons.

identification of the stress biomarker (cortisol: steroid hormone) by using antibody-functionalized tubular micromotors.[143] Fig. 8A indicates the detection of cortisol by the dynamic motors. The micromotors were functionalized with ani-cortisol antibody to detect the horseradish peroxidase (HRP)-labeled cortisol in the sample. It also demonstrated the rapid naked-eye detection of cortisol in the TMB/peroxide medium. The conversion of the color of TMB solution from light to dark blue shows the simple colorimetric assay in relation to the detection of cortisol in the presence of micromotors. The efficient fluid mixing induced by the micromotors assisted the quick detection of cortisol within 2 min, using a very small amount of sample (50 μL). This new concept can be extended for the easy and quick biomedical screening of cortisol by avoiding the need for laborious protocols.

To the best of our knowledge, the first example of cancer biomarker detection via protein molecules (Ab2 GMA) was done by Yu et al. in 2014 by utilizing gold nanoparticle-functionalized self-propelled polyaniline/Pt (AuNP/PANI/Pt) micromotors.[139] These biocompatible micromotors accelerated the immunoassay within 5 min, obviating the washing and separation step. Later, the group of Wang fabricated molybdenum disulfide-based tubular micro rockets for the sensing of a cancer biomarker. These 2D MoS₂/Pt micromotors exhibited rapid and sensitive fluorescence-based detection ability towards both protein (thrombin) and nucleic acid (micro-RNA 21) cancer biomarkers.[65] The micromotors were immobilized with fluorescent dye-labeled single-stranded DNA (FAM-ssDNA) and fluorescein isothiocyanate (FITC)-aptamer for the specific recognition of miRNA-21 and thrombin, respectively. When FAM-ssDNA or FITC-aptamer was attached to the surface of MoS₂, it resulted in rapid fluorescence quenching. The addition of complimentary miRNA-21 or thrombin

to the micromotor-containing solution caused the specific interaction of the dye-labeled DNA or aptamer with the added molecules. This event led to the release of the receptor units from the surface of the tubular micro-engine, and hence recovery of the fluorescence signal (Fig. 8B). The real-time fluorescent "OFF–ON" event is shown in Fig. 8B(b and c) for the static and mobile motors, respectively. It depicted the event of quenching-recovery for both target biomarkers without and with peroxide fuel. In mi-RNA detection, the dynamic micromotors successfully recovered about 96% signal, which was 6% for their static counterparts. On the contrary, they rendered 90% and 10% signal recovery for the motile and static motors for the detection of thrombin, respectively.

Currently, the widespread rise in diabetes has become a global concern.[140] According to data from the WHO, more than 400 million people are living with diabetes and 1.5 million people are dying annually due to this disease. Therefore, the precise detection of diabetes biomarkers (blood sugar) is crucial for regular monitoring of this disease. Motion-enhanced diffusion and electrogenerated chemiluminescence with enzyme-modified micromotors have succeeded in glucose biosensing.[141,142] Nevertheless, these motors rely on complex structural modification and show the inability to propel themselves in a viscoelastic medium. Hence, this limits the use of these motors in practical bio-media such as blood.

Thus, to address this problem, Kong et al. developed Mg/Pt biocompatible spherical microrobots for the accurate detection of glucose biomolecules in human serum.[144] The choice of these materials was attributed to the marvelous haemocompatibility of Mg and the inert nature of Pt. In addition, these micromotors exhibited fast motion in the viscous medium by the bubble recoil mechanism. The electrochemical detection of glucose by

Fig. 8 Schematic representation of biomarker detection. (A) Anti-cortisol-modified PEDOT/Ni/Pt micromotors for the ''on-the-fly'' detection of cortisol-HRP and micromotor-assisted naked-eye colorimetric assay in the presence of peroxide and TMB medium. Absorption spectra: sample without having cortisol-HRP (light blue line: transparent solution) and with cortisol-HRP (dark blue: blue color solution). Reproduced with permission from ref. 143 Copyright 2017, Elsevier. (B) Fluorescence ''OFF−ON'' detection of cancer biomarker (mi-RNA 21 and thrombin) by MoS$_2$/Pt-tubular micromotors. (a) Schematic of fluorescence quenching phenomenon upon the immobilization of FAM-ssDNA or FITC-aptamer and recovery of the signal due to the specific sensing of mi-RNA 21 or thrombin. (b and c) Real-time fluorescence images showing the time lapse study of quenching-recovery events for static (i and j) and motile micromotors (k and l) towards the detection of miRNA-21 and thrombin, respectively. Reproduced with permission from ref. 65 Copyright 2016, John Wiley and Sons. (C) Mg/Pt Janus micromotor-assisted electrochemical detection of glucose in human serum sample based on screen-printed electrode (SPE). Reproduced with permission from ref. 144 Copyright 2019, the American Chemical Society. (D) Smartphone-based strategy for motion-based sensing of glutathione (GSH) by GO-wrapped/PtNP Janus micromotors and plot signifies the linear fall in the speed of micromotors with respect to the concentration of target biomarker. Reproduced with permission from ref. 40 under CC-BY 4.0 License. Copyright 2021, the American Chemical Society.

the Mg/Pt motors is depicted in Fig. 8C. The detection platform was based on a screen-printed electrode, which was functionalized with the glucose oxidase (Gox) enzyme and ferrocene methanol (FcMeOH) to facilitate the electrochemical reaction. The fluid mixing and enhanced mass transfer by the micromotors played an important role in strengthening the electrochemical signal to determine the concertation of glucose in the human serum sample. The assistance of Janus motors in the enzymatic breakdown of glucose by GOx and interconversion of FcMeOH to Fc$^+$MeOH improved the current signal, and consequently the detection of even the slightest (millimolar) amount of glucose was possible. Thus, micromotor-assisted sensing can open a new door towards the rapid detection of glucose and other biomolecules at the clinically relevant level in the near future.

Glutathione is a crucial biomarker that plays a vital role in cellular functions and nutrient metabolism.[145,146] It is a peptide

biomolecule that gives the indication of many diseases such as viral infections, diabetes, and Alzheimer's disease.[147,148] A smartphone-based Janus micromotors strategy was adopted by Yuan *et al.* for the assessment of the motion-based detection of glutathione. They designed graphene oxide-wrapped polystyrene-gold Janus particles (20 μm diameter) with Pt nanoparticles (NPs) on the surface for the detection of the GSH biomarker.[40] When functionalized with thiol (-SH) and pipetted into GSH-rich medium, the catalytic activity of the micromotors was suppressed due to the attachment of GSH to thiol group. The catalytic activity of the micromotors is attributed to the Pt NPs present on the thiol-functionalized gold surface. The thiol group on the micromotors has specific affinity towards GSH. Thus, upon GSH attachment, the catalytic activity of the active Pt NPs was reduced, resulting in a significant reduction in the speed of the micromotors, as shown in Fig. 8D. The graphs interpreted the decrease in the speed of the

Table 3 Micromotors for biomolecule and biomarker sensing

Name of micro/nano-motors with size	Materials	Target	Sensing mechanism	Limit of detection	Author (year)
Biomolecules					
Tubular	PEDOT–Au	DNA	Motion-based detection (speed enhancement)	—	Van Nguyen et al.[149] (2015)
Tubular and ~13.5 µm length	PEDOT-PSS/Au	DNA	DNA displacement hybridization (speed reduction)	10 nM	Fu et al.[138] (2017)
Jellyfish and 20 µm opening size with 300 nm thickness	Au/Ag/Ni/Au	DNA	DNA displacement hybridization (speed reduction)	—	Zhang et al.[55] (2019)
Tubular and ~10 µm length	IrO$_2$/Pt	Protein (rabbit IgG)	Electrochemical detection	0.94 pg mL^{-1}	C. Mayorga-Martinez et al.[137] (2020)
Biomarkers					
Tubular and 5 µm length	Polyaniline (PANI)-Pt	Apolipoprotein E (alzheimer's disease biomarker)	Fluorescence detection	0.91 ng mL^{-1}	Morales-Narváez et al.[150] (2014)
Tubular	AuNP/PANI/Pt	Ab2-GMA (cancer biomarker)	Motion-based sensing (speed reduction)	—	Yu et al.[139] (2014)
Tubular and ~15 µm length	ssDNA@MoS$_2$/Pt and aptamer MoS$_2$/Pt	Nucleic acids: miRNA-21 and proteins: thrombin (cancer biomarker)	Fluorescence recovery	—	V. Singh et al.[65] (2016)
Tubular and 10 µm length	Au-sputtered PEDOT/Ni/Pt	Cortisol (stress and clinical biomarker)	Colorimetric sensing	0.1 µg L^{-1}	Esteban-Fernández de Ávila et al.[143] (2017)
Spherical and 1 µm diameter	Multifunctional magnetic bead	Procalcitonin (sepsis biomarker)	Colorimetric sensing	2 ng mL^{-1}	M. Russell et al.[67] (2019)
Spherical and 20 µm diameter	Mg/Pt	Glucose (diabetes biomarker)	Electrochemical sensing	33.2 µM (1 mg mL^{-1} of micromotors)	Kong et al.[144] (2019)
Tubular and 12.6 µm length	electrochemically reduced graphene oxide (erGO)/Pt	Reprimo (gastric cancer biomarker)	Fluorescence recovery	1.3 µM	F. Báez et al.[151] (2020)
Tubular and 20 µm length	PPy(polypyrrole)/Ni/PtNP	Procalcitonin (sepsis biomarker)	Fluorescence detection	0.07 ng mL^{-1}	Molinero-Fernandez et al.[152] (2020)
Tubular and 10 µm length	rGO/Ni/PtNPs	C-Reactive protein (sepsis biomarker)	Electrochemical detection	0.80 µg mL^{-1}	Molinero-Fernandez et al.[39] (2020)
Tubular and 11.75 µm length	Au/PEDOT/Pt	miRNA-21 (cancer biomarker)	Fluorescence quenching	—	Yurdabak Karaca et al.[153] (2021)
Tubular and ~10 µm length	Au/Pt bimetallic	miRNA-21 (cancer biomarker)	Fluorescence quenching	0.41 nM w/o and 0.19 nM with surface acoustic wave forces	Celik Cogal et al.[45] (2021)
Spherical Janus and 20 µm diameter	GO/PtNP	Glutathione (peptide biomarker related to Alzheimer's disease, viral infection)	Motion-based sensing (speed reduction)	0.90 µM	Yuan et al.[40] (2021)

micromotors upon detection of GSH with an increase in the concentration of GSH (10–160 µM). This reduction in speed (from a high value to almost zero) is attributed to the poisoning of the Pt catalyst due to the interaction with GSH, which stopped the catalytic decomposition of peroxide to produce oxygen bubbles for actuation. This group also tested the practical utility of these micromotors for GSH detection in a human serum sample with varying concentrations, which showed the superiority of the smartphone-based micromotor platform in disease monitoring associated with GSH and proved to be the most economical technique for the analysis of samples (blood) fortified with this biomarker.

A detailed summary of the sensing of biomolecules and biomarkers is highlighted in Table 3.

5. Conclusions and future perspectives

In this review, we discussed and presented the bubble-propelled micromotors employed for sensing hazardous pollutants and biological agents. Initially, we highlighted the various structures of bubble-powered micromotors and their mechanism of sensing. Basically, four detection strategies and their connection to environmental pollutant detection and biosensing were revealed. In the next sections, how the bubble-powered motion shows efficacy in the application of "on-the-fly" sensing ranging from the detection of a myriad of inorganic and organic environmental pollutants and bio-analytes was explained step by step. According to our highlighted figures and summarised tabulated data, we showed that micromotors employ different inorganic materials such as Pt, Ag, Ir, Mg, and Mn$_2$O$_3$ and the enzyme catalase for bubble propulsion. Among these materials, most of the micromotors relied on Pt and some used catalase as the power unit. The reason for the choice of Pt as a catalyst among the inorganic materials is due to its non-toxicity, resistance to corrosion, and the longer operational period during the catalytic reaction. Besides Pt, micromotors modified with catalase were successful in different proof-of-concept applications ranging from the environmental field such as gas sensing to biosensing.

Although these motors show supremacy in analytical sensing, they still exhibit some major limitations. The majority of micromotors are fuel-based, which needs toxic fuel such as peroxide and sodium dodecyl sulfate for actuation. Thus, this chemical fuel-based aqueous medium will not only affect the intrinsic property of the sensing environment but also limit the motion of the micromotors to a short period. Moreover, it may hinder their usability in real bio-medium owing to their non-biocompatible nature. A few reports suggested that materials such as Mg, Zn, Al, and enzymes such as catalase, urease, and glucose oxidase require no peroxide medium for propulsion based on the bubble propulsion mechanism.[47] For instance, Mg/Zn-based micromotors have been successfully employed for *in vivo* use by generating hydrogen bubbles in gastric acid medium.[154,155] Similarly, Mg, Al-like materials were driven in water medium by the generation of bubbles.[47,156] Hence, they can be alternative choices of fuel medium for the realization of the practical application of micromotors. Secondly, many groups checked the performance of micromotors in the selective detection of targets, but none carefully addressed the resolution and sensing accuracy of the micromotors in detail. Hence, high accuracy with better resolution is necessary to make micromotors comparable with the traditional characterization techniques. Briefly, to realize the ability of these motors for *in vivo* sensing, the choice of materials, medium of propulsion, biocompatibility, selectivity, resolution of sensing, and study under all the crucial environmental parameters must be highlighted.

Despite all the challenges and hurdles, the emerging field of bubble-powered micromotor platforms has successfully brought novelty and revolutionized the field of sensing. However, we are anticipating the fuel-free operation of micromotors with a good limit of detection and resolution, which will dominate the field of sensing in the near future. Additionally, it will be a tough task for researchers to make biocompatible microrobots available on a large scale with low-cost optical visualization and portable set up worldwide to solve real-life problems. Thus, scientists must conduct a thorough investigation before choosing the materials and focus on reliable and economical fabrication steps to ensure the easy accessibility of these motors or techniques to all research laboratories of low- and middle-income countries. This will not only promote their use but also create an awareness of this type of existing technology. Simultaneously, intense research will be required for the optimization of micromotor design and concentration of fuel medium to ensure biocompatibility and to apply the micromotors for *in vivo* sensing. If this is possible for rapid sensing at the cellular level and complex biological environment within a few years, then it definitely will bring dramatic changes in the biomedical field for the real-time monitoring of various chronic ailments. The incorporation of these micro/nanomotors in sensing will promote the early detection of diseases and help in monitoring toxic environmental pollutants and food poisoning. Early diagnosis will reduce the mortality rates and fasten the treatment process without the necessity of high cost. This comprehensive review may excite researchers and shed light to illuminate their path for the exploration and development of micromotors for environmental pollutant detection and diagnostic sensing. Considering all the advantages and drawbacks, it can be concluded that micromotor-assisted sensing will be a potential next-generation environmental and biomedical probing tool, but currently, it is in its infancy, and it will probably take another 10 to 15 years to be partially or fully optimized for effective use in real situations.

Conflicts of interest

The authors declare that they have no conflicts of interest.

Acknowledgements

References

1 Q. Wang and Z. Yang, *Environ. Pollution*, 2016, **218**, 358–365.
2 M. M. Khin, A. S. Nair, V. J. Babu, R. Murugan and S. Ramakrishna, *Energy Environ. Sci.*, 2012, **5**, 8075.
3 R. P. Schwarzenbach, T. Egli, T. B. Hofstetter, U. von Gunten and B. Wehrli, *Annu. Rev. Environ. Resour.*, 2010, **35**, 109–136.
4 Y. Zhang, K. Yuan and L. Zhang, *Adv. Mater. Technol.*, 2019, **4**, 1800636.
5 K. M. Aguilar-Pérez, M. S. Heya, R. Parra-Saldívar and H. M. N. Iqbal, *Case Stud. Chem. Environ. Eng.*, 2020, **2**, 100055.
6 R. C. Barry, Y. Lin, J. Wang, G. Liu and C. A. Timchalk, *J. Exposure Sci. Environ. Epidemiol.*, 2009, **19**, 1–18.
7 H. Kumar, K. Kuča, S. K. Bhatia, K. Saini, A. Kaushal, R. Verma, T. C. Bhalla and D. Kumar, *Sensors*, 2020, **20**, 1966.
8 S. Sharma and M. Madou, *Philos. Trans. R. Soc., A*, 2012, **370**, 2448–2473.
9 M. Cheng, G. Cuda, Y. Bunimovich, M. Gaspari, J. Heath, H. Hill, C. Mirkin, A. Nijdam, R. Terracciano and T. Thundat, *Curr. Opin. Chem. Biol.*, 2006, **10**, 11–19.
10 X. Zhang, Q. Guo and D. Cui, *Sensors*, 2009, **9**, 1033–1053.
11 M. Vaculovicova, P. Michalek, S. Krizkova, M. Macka and V. Adam, *Anal. Methods*, 2017, **9**, 2375–2391.
12 H.-H. Jeong, A. G. Mark, M. Alarcón-Correa, I. Kim, P. Oswald, T.-C. Lee and P. Fischer, *Nat. Commun.*, 2016, **7**, 11331.
13 M. Zarei and M. Zarei, *Small*, 2018, **14**, 1800912.
14 M. Pacheco, M. Á. López, B. Jurado-Sánchez and A. Escarpa, *Anal. Bioanal. Chem.*, 2019, **411**, 6561–6573.
15 B. Jurado-Sánchez, *Biosensors*, 2018, **8**, 59.
16 B. Jurado-Sánchez and A. Escarpa, *Electroanalysis*, 2017, **29**, 14–23.

17 B. Jurado-Sánchez, S. Campuzano, J. M. Pingarrón and A. Escarpa, *Microchim. Acta*, 2021, **188**, 416.

18 L. Kong, J. Guan and M. Pumera, *Curr. Opin. Electrochem.*, 2018, **10**, 174–182.

19 S. Palagi, D. P. Singh and P. Fischer, *Adv. Opt. Mater.*, 2019, **7**, 1900370.

20 D. P. Singh, W. E. Uspal, M. N. Popescu, L. G. Wilson and P. Fischer, *Adv. Funct. Mater.*, 2018, **28**, 1706660.

21 D. P. Singh, U. Choudhury, P. Fischer and A. G. Mark, *Adv. Mater.*, 2017, **29**, 1701328.

22 S. Debata, N. A. Kherani, S. K. Panda and D. P. Singh, *J. Mater. Chem. B*, 2022, **10**, 8235–8243.

23 J. Yan, M. Han, J. Zhang, C. Xu, E. Luijten and S. Granick, *Nat. Mater.*, 2016, **15**, 1095–1099.

24 S. Gangwal, O. J. Cayre, M. Z. Bazant and O. D. Velev, *Phys. Rev. Lett.*, 2008, **100**, 058302.

25 C.-H. Lin, Y.-L. Chen and H.-R. Jiang, *RSC Adv.*, 2017, **7**, 46118–46123.

26 X. Lu, H. Shen, K. Zhao, Z. Wang, H. Peng and W. Liu, *Chem. – Asian J.*, 2019, **14**, 2406–2416.

27 L. Ren, W. Wang and T. E. Mallouk, *Acc. Chem. Res.*, 2018, **51**, 1948–1956.

28 P. Fischer and A. Ghosh, *Nanoscale*, 2011, **3**, 557–563.

29 P. Mandal, G. Patil, H. Kakoty and A. Ghosh, *Acc. Chem. Res.*, 2018, **51**, 2689–2698.

30 P. L. Venugopalan and A. Ghosh, *Langmuir*, 2021, **37**, 289–296.

31 X. Chen, C. Zhou and W. Wang, *Chem. – Asian J.*, 2019, **14**, 2388–2405.

32 A. Somasundar and A. Sen, *Small*, 2021, **17**, 2007102.

33 Z. H. Shah, S. Wang, L. Xian, X. Zhou, Y. Chen, G. Lin and Y. Gao, *Chem. Commun.*, 2020, **56**, 15301–15304.

34 M. Safdar, O. M. Wani and J. Jänis, *ACS Appl. Mater. Interfaces*, 2015, **7**, 25580–25585.

35 H. Wang and M. Pumera, *Chem. Rev.*, 2015, **115**, 8704–8735.

36 B. Esteban-Fernández de Ávila, M. A. Lopez-Ramirez, D. F. Báez, A. Jodra, V. V. Singh, K. Kaufmann and J. Wang, *ACS Sens.*, 2016, **1**, 217–221.

37 M. S. Draz, N. K. Lakshminaraasimulu, S. Krishnakumar, D. Battalapalli, A. Vasan, M. K. Kanakasabapathy, A. Sreeram, S. Kallakuri, P. Thirumalaraju, Y. Li, S. Hua, X. G. Yu, D. R. Kuritzkes and H. Shafiee, *ACS Nano*, 2018, **12**, 5709–5718.

38 J. Wu, S. Balasubramanian, D. Kagan, K. M. Manesh, S. Campuzano and J. Wang, *Nat. Commun.*, 2010, **1**, 36.

39 Á. Molinero-Fernández, M. Á. López and A. Escarpa, *Anal. Chem.*, 2020, **92**, 5048–5054.

40 K. Yuan, C. Cuntín-Abal, B. Jurado-Sánchez and A. Escarpa, *Anal. Chem.*, 2021, **93**, 16385–16392.

41 L. Baraban, M. Tasinkevych, M. N. Popescu, S. Sanchez, S. Dietrich and O. G. Schmidt, *Soft Matter*, 2012, **8**, 48–52.

42 W. He, J. Frueh, N. Hu, L. Liu, M. Gai and Q. He, *Adv. Sci.*, 2016, **3**, 1600206.

43 M. Guix, S. M. Weiz, O. G. Schmidt and M. Medina-Sánchez, *Part. Part. Syst. Charact.*, 2018, **35**, 1700382.

44 A. A. Solovev, S. Sanchez, M. Pumera, Y. F. Mei and O. G. Schmidt, *Adv. Funct. Mater.*, 2010, **20**, 2430–2435.

45 G. Celik Cogal, P. K. Das, G. Yurdabak Karaca, V. R. Bhethanabotla and A. Uygun Oksuz, *ACS Appl. Bio Mater.*, 2021, **4**, 7932–7941.

46 W. Gao, A. Uygun and J. Wang, *J. Am. Chem. Soc.*, 2012, **134**, 897–900.

47 Q. Chi, Z. Wang, F. Tian, J. You and S. Xu, *Micromachines*, 2018, **9**, 537.

48 J. Orozco, B. Jurado-Sánchez, G. Wagner, W. Gao, R. Vazquez-Duhalt, S. Sattayasamitsathit, M. Galarnyk, A. Cortés, D. Saintillan and J. Wang, *Langmuir*, 2014, **30**, 5082–5087.

49 J. G. Gibbs and Y.-P. Zhao, *Appl. Phys. Lett.*, 2009, **94**, 163104.

50 Y. Ge, M. Liu, L. Liu, Y. Sun, H. Zhang and B. Dong, *Nano-Micro Lett.*, 2016, **8**, 157–164.

51 S. Park and G. Yossifon, *ACS Sens.*, 2020, **5**, 936–942.

52 Q. Zhang, R. Dong, Y. Wu, W. Gao, Z. He and B. Ren, *ACS Appl. Mater. Interfaces*, 2017, **9**, 4674–4683.

53 B. Esteban-Fernández de Ávila, A. Martín, F. Soto, M. A. Lopez-Ramirez, S. Campuzano, G. M. Vásquez-Machado, W. Gao, L. Zhang and J. Wang, *ACS Nano*, 2015, **9**, 6756–6764.

54 D. Zhang, D. Wang, J. Li, X. Xu, H. Zhang, R. Duan, B. Song, D. Zhang and B. Dong, *J. Mater. Sci.*, 2019, **54**, 7322–7332.

55 X. Zhang, C. Chen, J. Wu and H. Ju, *ACS Appl. Mater. Interfaces*, 2019, **11**, 13581–13588.

56 M. Pacheco, V. de la Asunción-Nadal, B. Jurado-Sánchez and A. Escarpa, *Biosens. Bioelectron.*, 2020, **165**, 112286.

57 W. Yang, J. Li, Z. Xu, J. Yang, Y. Liu and L. Liu, *J. Mater. Chem. C*, 2019, **7**, 10297–10308.

58 M. Liu, Y. Sun, T. Wang, Z. Ye, H. Zhang, B. Dong and C. Y. Li, *J. Mater. Chem. C*, 2016, **4**, 5945–5952.

59 Y. Yuan, C. Gao, D. Wang, C. Zhou, B. Zhu and Q. He, *Beilstein J. Nanotechnol.*, 2019, **10**, 1324–1331.

60 M. Cerruti, J. Jaworski, D. Raorane, C. Zueger, J. Varadarajan, C. Carraro, S.-W. Lee, R. Maboudian and A. Majumdar, *Anal. Chem.*, 2009, **81**, 4192–4199.

61 T. Kawaguchi, D. R. Shankaran, S. J. Kim, K. Matsumoto, K. Toko and N. Miura, *Sens. Actuators, B*, 2008, **133**, 467–472.

62 D. Gao, Z. Wang, B. Liu, L. Ni, M. Wu and Z. Zhang, *Anal. Chem.*, 2008, **80**, 8545–8553.

63 Z. Shen, A. Wu and X. Chen, *Chem. Soc. Rev.*, 2017, **46**, 2038–2056.

64 L. Zhao, Y. Liu, S. Xie, P. Ran, J. Wei, Q. Liu and X. Li, *Chem. Eng. J.*, 2020, **382**, 123041.

65 V. V. Singh, K. Kaufmann, B. E.-F. de Ávila, E. Karshalev and J. Wang, *Adv. Funct. Mater.*, 2016, **26**, 6270–6278.

66 K. Wang, E. Ma, Z. Hu and H. Wang, *Chem. Commun.*, 2021, **57**, 10528–10531.

67 S. M. Russell, A. Alba-Patiño, M. Borges and R. de la Rica, *Biosens. Bioelectron.*, 2019, **140**, 111346.

68 V. V. Singh, K. Kaufmann, J. Orozco, J. Li, M. Galarnyk, G. Arya and J. Wang, *Chem. Commun.*, 2015, **51**, 11190–11193.

69 J. Yang, J. Li, X. Yan, Y. Lyu, N. Xing, P. Yang, P. Song and M. Zuo, *ACS Appl. Mater. Interfaces*, 2022, **14**, 6484–6498.

70 B. Jurado-Sánchez, M. Pacheco, R. Maria-Hormigos and A. Escarpa, *Appl. Mater. Today*, 2017, **9**, 407–418.

71 Y. Ye, J. Luan, M. Wang, Y. Chen, D. A. Wilson, F. Peng and Y. Tu, *Chem. – Eur. J.*, 2019, **25**, 8663–8680.

72 S. Kumar and R. Singh, *Opt. Laser Technol.*, 2021, **134**, 106620.

73 Y. Zhang, K. Yan, F. Ji and L. Zhang, *Adv. Funct. Mater.*, 2018, **28**, 1806340.

74 J. Parmar, D. Vilela, K. Villa, J. Wang and S. Sánchez, *J. Am. Chem. Soc.*, 2018, **140**, 9317–9331.

75 H. Ali, E. Khan and I. Ilahi, *J. Chem.*, 2019, **2019**, 1–14.

76 P. B. Tchounwou, C. G. Yedjou, A. K. Patlolla and D. J. Sutton, in *Molecular, Clinical and Environmental Toxicology*, ed. A. Luch, Springer Basel, Basel, 2012, vol. 101, pp. 133–164.

77 L. Chen, S. Zhou, Y. Shi, C. Wang, B. Li, Y. Li and S. Wu, *Sci. Total Environ.*, 2018, **615**, 141–149.

78 P. E. Paus, *Z. Anal. Chem.*, 1973, **264**, 118–122.

79 M. Ghaedi, M. Reza Fathi, A. Shokrollahi and F. Shajarat, *Anal. Lett.*, 2006, **39**, 1171–1185.

80 Y. Wing Fen and W. Mahmood Mat Yunus, *Sens. Rev.*, 2013, **33**, 305–314.

81 S. Wang, E. S. Forzani and N. Tao, *Anal. Chem.*, 2007, **79**, 4427–4432.

82 R. M. Abdul, L. Mutnuri, P. J. Dattatreya and D. A. Mohan, *Environ. Monit. Assess.*, 2012, **184**, 1581–1592.

83 G. Xing, M. R. Sardar, B. Lin and J.-M. Lin, *Talanta*, 2019, **204**, 50–56.

84 L.-G. Danielsson, B. Magnusson and S. Westerlund, *Anal. Chim. Acta*, 1978, **98**, 47–57.

85 S. T. Palisoc, R. I. M. Vitto, M. G. Noel, K. T. Palisoc and M. T. Natividad, *Sci. Rep.*, 2021, **11**, 1394.

86 Q. Hu, G. Yang, Y. Zhao and J. Yin, *Anal. Bioanal. Chem.*, 2003, **375**, 831–835.

87 B. Jurado-Sánchez, A. Escarpa and J. Wang, *Chem. Commun.*, 2015, **51**, 14088–14091.

88 D. Kagan, P. Calvo-Marzal, S. Balasubramanian, S. Sattayasamitsathit, K. M. Manesh, G.-U. Flechsig and J. Wang, *J. Am. Chem. Soc.*, 2009, **131**, 12082–12083.

89 F. N. Diauudin, J. I. A. Rashid, V. F. Knight, W. M. Z. Wan Yunus, K. K. Ong, N. A. M. Kasim, N. Abdul Halim and S. A. M. Noor, *Sens. Bio-Sens. Res.*, 2019, **26**, 100305.

90 W. E. Steiner, S. J. Klopsch, W. A. English, B. H. Clowers and H. H. Hill, *Anal. Chem.*, 2005, **77**, 4792–4799.

91 S. Choi, Y. Jeong, Y. J. Koh, J. H. Lee, H. Nam and J. Lee, *Bull. Korean Chem. Soc.*, 2019, **40**, 279–284.

92 L. M. Matz, P. S. Tornatore and H. H. Hill, *Talanta*, 2001, **54**, 171–179.

93 H. Sohn, S. Létant, M. J. Sailor and W. C. Trogler, *J. Am. Chem. Soc.*, 2000, **122**, 5399–5400.

94 V. V. Singh, P. K. Sharma, A. Shrivastava, P. K. Gutch, K. Ganesan and M. Boopathi, *Electroanalysis*, 2020, **32**, 1671–1680.

95 W. Lu, Y. Ni, G. Jia, H. Pan and C. Zhao, *Asian J. Chem.*, 2014, **26**, 773–776.

96 V. V. Singh and J. Wang, *Nanoscale*, 2015, **7**, 19377–19389.

97 K. Wang, W. Wang, S. Pan, Y. Fu, B. Dong and H. Wang, *Appl. Mater. Today*, 2020, **19**, 100550.

98 K. Borgå, *Reference Module in Earth Systems and Environmental Sciences*, Elsevier, 2013, p. B978012409548900765X.

99 R. Dong, J. Li, I. Rozen, B. Ezhilan, T. Xu, C. Christianson, W. Gao, D. Saintillan, B. Ren and J. Wang, *Sci. Rep.*, 2015, **5**, 13226.

100 J. Orozco, V. García-Gradilla, M. D'Agostino, W. Gao, A. Cortés and J. Wang, *ACS Nano*, 2013, **7**, 818–824.

101 J. G. S. Moo, H. Wang, G. Zhao and M. Pumera, *Chem. – Eur. J.*, 2014, **20**, 4292–4296.

102 B. Jurado-Sánchez, J. Wang and A. Escarpa, *ACS Appl. Mater. Interfaces*, 2016, **8**, 19618–19625.

103 K. Villa, C. L. Manzanares Palenzuela, Z. Sofer, S. Matějková and M. Pumera, *ACS Nano*, 2018, **12**, 12482–12491.

104 T. Maric, C. C. Mayorga-Martinez, M. Z. M. Nasir and M. Pumera, *Adv. Mater. Technol.*, 2019, **4**, 1800502.

105 T. Li, Y. Lyu, J. Li, C. Wang, N. Xing, J. Yang and M. Zuo, *Environ. Sci.: Nano*, 2021, **8**, 3833–3845.

106 W. Yang, J. Li, Y. Lyu, X. Yan, P. Yang and M. Zuo, *J. Cleaner Prod.*, 2021, **309**, 127294.

107 S. Cinti, G. Valdés-Ramírez, W. Gao, J. Li, G. Palleschi and J. Wang, *Chem. Commun.*, 2015, **51**, 8668–8671.

108 V. V. Singh, K. Kaufmann, B. Esteban-Fernández de Ávila, M. Uygun and J. Wang, *Chem. Commun.*, 2016, **52**, 3360–3363.

109 D. Rojas, B. Jurado-Sánchez and A. Escarpa, *Anal. Chem.*, 2016, **88**, 4153–4160.

110 R. María-Hormigos, B. Jurado-Sánchez and A. Escarpa, *Anal. Chem.*, 2018, **90**, 9830–9837.

111 S. Vigneshvar, C. C. Sudhakumari, B. Senthilkumaran and H. Prakash, *Front. Bioeng. Biotechnol.*, 2016, **4**, DOI: 10.3389/fbioe.2016.00011.

112 R. de la Rica and M. M. Stevens, *Nat. Nanotechnol.*, 2012, **7**, 821–824.

113 J. Verma, S. Saxena and S. G. Babu, in *Analyzing Microbes: Manual of Molecular Biology Techniques*, ed. D. K. Arora, S. Das and M. Sukumar, Springer Berlin Heidelberg, Berlin, Heidelberg, 2013, pp. 169–186.

114 S. Hosseini, P. Vázquez-Villegas, M. Rito-Palomares and S. O. Martinez-Chapa, in *Enzyme-linked Immunosorbent Assay (ELISA): From A to Z*, ed. S. Hosseini, P. Vázquez-Villegas, M. Rito-Palomares and S. O. Martinez-Chapa, Springer Singapore, Singapore, 2018, pp. 31–56.

115 C. Wei, M. Li and X. Zhao, *Front. Microbiol.*, 2018, **9**, DOI: 10.3389/fmicb.2018.02857.

116 L. Li, M. Liao, Y. Chen, B. Shan and M. Li, *J. Mater. Chem. B*, 2019, **7**, 815–822.

117 Y. Yamamoto, *Clin. Vaccine Immunol.*, 2002, **9**, 508–514.

118 H. Cheng, W. He, J. Yang, Q. Ye, L. Cheng, Y. Pan, L. Mao, X. Chu, C. Lu, G. Li, Y. Qiu and J. He, *Cell Proliferation*, 2020, **53**, e12880.

119 M. Gerhard, H. Juhl, H. Kalthoff, H. W. Schreiber, C. Wagener and M. Neumaier, *JCO*, 1994, **12**, 725–729.

120 J. E. Olsen, S. Aabo, W. Hill, S. Notermans, K. Wernars, P. E. Granum, T. Popovic, H. N. Rasmussen and Ø. Olsvik, *Int. J. Food Microbiol.*, 1995, **28**, 1–78.

121 Á. Molinero-Fernández, M. Moreno-Guzmán, M. Á. López and A. Escarpa, *Anal. Chem.*, 2017, **89**, 10850–10857.

122 S. Hammerschmidt, J. Hacker and H.-D. Klenk, *Int. J. Med. Microbiol.*, 2005, **295**, 141–151.

123 M. Tubiana, *Acta Oncol.*, 1989, **28**, 113–121.

124 B. Jurado-Sánchez, M. Pacheco, J. Rojo and A. Escarpa, *Angew. Chem., Int. Ed.*, 2017, **56**, 6957–6961.

125 E. Antoniou, E. Orovou, A. Sarella, M. Iliadou, N. Rigas, E. Palaska, G. Iatrakis and M. Dagla, *IJERPH*, 2020, **17**, 3806.

126 M. S. Draz, K. M. Kochehbyoki, A. Vasan, D. Battalapalli, A. Sreeram, M. K. Kanakasabapathy, S. Kallakuri, A. Tsibris, D. R. Kuritzkes and H. Shafiee, *Nat. Commun.*, 2018, **9**, 4282.

127 X. Guan, *Acta Pharm. Sin. B*, 2015, **5**, 402–418.

128 V. Plaks, C. D. Koopman and Z. Werb, *Science*, 2013, **341**, 1186–1188.

129 Z. Zhang, J. Li, L. Fu, D. Liu and L. Chen, *J. Mater. Chem. A*, 2015, **3**, 7437–7444.

130 M. Pacheco, B. Jurado-Sánchez and A. Escarpa, *Anal. Chem.*, 2018, **90**, 2912–2917.

131 L. Zhao, S. Xie, Y. Liu, Q. Liu, X. Song and X. Li, *Nanoscale*, 2019, **11**, 17831–17840.

132 V. de la Asunción-Nadal, M. Pacheco, B. Jurado-Sánchez and A. Escarpa, *Anal. Chem.*, 2020, **92**, 9188–9193.

133 K. Yuan, M. Á. López, B. Jurado-Sánchez and A. Escarpa, *ACS Appl. Mater. Interfaces*, 2020, **12**, 46588–46597.

134 M. Pacheco, B. Jurado-Sánchez and A. Escarpa, *Microchim. Acta*, 2022, **189**, 194.

135 Á. Molinero-Fernández, A. Jodra, M. Moreno-Guzmán, M. Á. López and A. Escarpa, *Chem. – Eur. J.*, 2018, **24**, 7172–7176.

136 A. Taj, A. Rehman and S. Z. Bajwa, in *Nanobiosensors*, ed. A. Wu and W. S. Khan, Wiley, 1st edn, 2020, pp. 73–94.

137 C. C. Mayorga-Martinez and M. Pumera, *Adv. Funct. Mater.*, 2020, **30**, 1906449.

138 S. Fu, X. Zhang, Y. Xie, J. Wu and H. Ju, *Nanoscale*, 2017, **9**, 9026–9033.

139 X. Yu, Y. Li, J. Wu and H. Ju, *Anal. Chem.*, 2014, **86**, 4501–4507.

140 X. Lin, Y. Xu, X. Pan, J. Xu, Y. Ding, X. Sun, X. Song, Y. Ren and P.-F. Shan, *Sci. Rep.*, 2020, **10**, 14790.

141 A.-I. Bunea, I.-A. Pavel, S. David and S. Gáspár, *Biosens. Bioelectron.*, 2015, **67**, 42–48.

142 M. Sentic, S. Arbault, B. Goudeau, D. Manojlovic, A. Kuhn, L. Bouffier and N. Sojic, *Chem. Commun.*, 2014, **50**, 10202–10205.

143 B. E.-F. de Ávila, M. Zhao, S. Campuzano, F. Ricci, J. M. Pingarrón, M. Mascini and J. Wang, *Talanta*, 2017, **167**, 651–657.

144 L. Kong, N. Rohaizad, M. Z. M. Nasir, J. Guan and M. Pumera, *Anal. Chem.*, 2019, **91**, 5660–5666.

145 G. K. Balendiran, R. Dabur and D. Fraser, *Cell Biochem. Funct.*, 2004, **22**, 343–352.

146 L. Hakuna, B. Doughan, J. O. Escobedo and R. M. Strongin, *Analyst*, 2015, **140**, 3339–3342.

147 N. Ballatori, S. M. Krance, S. Notenboom, S. Shi, K. Tieu and C. L. Hammond, *Biol. Chem.*, 2009, **390**, 191–214.

148 H. Liu, H. Wang, S. Shenvi, T. M. Hagen and R.-M. Liu, *Ann. N. Y. Acad. Sci.*, 2004, **1019**, 346–349.

149 K. Van Nguyen and S. D. Minteer, *Chem. Commun.*, 2015, **51**, 4782–4784.

150 E. Morales-Narváez, M. Guix, M. Medina-Sánchez, C. C. Mayorga-Martinez and A. Merkoçi, *Small*, 2014, **10**, 2542–2548.

151 D. F. Báez, G. Ramos, A. Corvalán, M. L. Cordero, S. Bollo and M. J. Kogan, *Sens. Actuators, B*, 2020, **310**, 127843.

152 Á. Molinero-Fernández, M. Moreno-Guzmán, L. Arruza, M. Á. López and A. Escarpa, *ACS Sens.*, 2020, **5**, 1336–1344.

153 G. Yurdabak Karaca, F. Kuralay, O. Bingol Ozakpinar, E. Uygun, U. Koc, S. Ulusoy, G. Bosgelmez Tinaz, L. Oksuz and A. Uygun Oksuz, *Appl. Nanosci.*, 2023, **13**, 367–367.

154 J. Li, S. Thamphiwatana, W. Liu, B. Esteban-Fernández de Ávila, P. Angsantikul, E. Sandraz, J. Wang, T. Xu, F. Soto, V. Ramez, X. Wang, W. Gao, L. Zhang and J. Wang, *ACS Nano*, 2016, **10**, 9536–9542.

155 W. Gao, R. Dong, S. Thamphiwatana, J. Li, W. Gao, L. Zhang and J. Wang, *ACS Nano*, 2015, **9**, 117–123.

156 W. Gao, A. Pei and J. Wang, *ACS Nano*, 2012, **6**, 8432–8438.